PROJECT TITLE, II -1	Gas Assisted Acidizing in Carbonate Reservoirs
PRINICIPAL INVESTIGATOR:	Dr. A. D. Hill
RESEARCH SCIENTIST:	Dr. D. Zhu
GRADUATE STUDENT:	Suneet Shukla

SUMMARY

Experiments carried out suggest that the volumes of acid required to propagate a wormhole in a carbonate rock after the injection of gas are less than the acid volumes required without any prior gas injection. It appears that the gas by reducing mobility in the rock surrounding the wormhole reduces fluid loss along the wormhole, leading to a more efficient transport of acid to the wormhole tip and faster wormhole propagation.

To improve the matrix acidizing process in carbonate reservoirs, we have carried out injection of an inert gas (nitrogen), either prior to the injected acid or simultaneously with the acid. We think this injection of gas increases the penetration of wormholes and improve the acid coverage in carbonate reservoirs.

We have conducted 4 series of experiments using an experimental setup in the lab. The setup comprises a core holder in which 6” x 1” cores are placed. First the cores are evacuated using a vacuum pump. Then, brine is pumped until the core becomes totally saturated. After that nitrogen is passed through at high pressure to bring the core to residual brine saturation. The last step of the experiment is to inject acid through the core.

We have conducted experiments without the injection of gas and then a series of experiments with gas injection and compared the volumes of acid used in each case. We compared the results in both cases for varying injection rates, temperature, and nature of fluid saturating the core prior to gas injection. These series of laboratory experiments with gas/acid injection will help to characterize the wormholing efficiency of the process. We have also made Wood’s metal castings of the wormholes obtained in the experiments to determine the morphology of the wormholes. In addition, we plan to model the acid placement when gas and acid are injected into a well penetrating a carbonate formation.

INTRODUCTION

WORMHOLING IN CARBONATE ACIDIZING

Matrix acidizing is a technique commonly used to enhance the production of oil or gas. It involves the injection of acid into a formation at a pressure below the fracture pressure of the reservoir. Acid dissolves the rock matrix near the wellbore, thus removing the formation damage caused by drilling or completion fluids and increasing the near wellbore permeability.

When carbonates are acidized using hydrochloric acid, the dissolution of rock matrix is not uniform as in sandstone acidizing. Instead, highly conductive flow channels known as wormholes result due to non-uniform dissolution. Thus, this highly selective pattern of dissolution dissolves certain parts of the medium creating infinitely permeable channels whereas other parts remain unaffected.

The structure of wormhole channels is strongly dependent on the rates of mass transfer and surface reaction, which may vary considerably among different acid / rock systems and also depend on flow geometry and injection rate. Since the wormholes are much larger than the pores the pressure drop through the region penetrated by wormholes will be insignificant. Thus, the effect of acidizing on the skin effect depends on the wormhole pattern, wormhole density, and wormhole penetration depth.

Wormholes form in a dissolution process when the large pores grow at a rate substantially higher than that at which the small pores grow, so that a large pore receives an increasingly larger portion of the dissolving fluid, eventually becoming a wormhole. As acid moves through a large pore or channel, acid moves to the reactive surface by molecular diffusion, but also by convective transport as acid flows to the small pores connected with the large pore. As the large pore grows, the fluid loss flux is a larger and larger portion of the transport of acid to the wormhole wall and is ultimately the limiting factor of wormhole growth. Thus, whether or not wormholes do form and the structure of wormholes that do form depends on the relative rate of surface reaction, diffusion and fluid loss, all of which depend on the overall injection rate of the acid.

The most efficient process is clearly the one that will create narrower wormholes with a minimum of branching and needs the least volume of acid to propagate the wormholes a

given distance. This process will enhance the near wellbore permeability to the greatest depth with the smallest volume of acid.

BACKGROUND OF THE PROJECT

The propagation of wormholes during carbonate acidizing has been studied extensively, both experimentally and theoretically. A key finding of the studies has been that the propagation of wormholes depends very strongly on the fluid loss out of the walls of the major wormholes. High fluid loss results in highly branched wormhole structures, which require much more acid to propagate a given distance than do wormholes having less fluid loss through the walls. In fact, the practical length of wormholes obtainable is limited by the fluid loss when the fluid loss becomes equal to the input, propagation ceases. Thus, processes that reduce the fluid loss from a wormhole will increase the efficiency of wormhole propagation (greater wormhole length for a given volume of acid injected). Fluids such as water in oil emulsions have been investigated for improved wormhole propagation in the past. However, a much simpler and less expensive approach may be to build a gas saturation around the wormholes. The reduced relative permeability to the aqueous phase will reduce the fluid loss from a wormhole propagating through a gas-saturated porous medium.

An additional potential benefit of gas injection for the carbonate acidizing process is diversion of acid to untreated intervals. Injection of gas into regions where wormholes have been created will increase resistance to subsequent slugs of acid because of reduced aqueous relative permeability. We will model this two-phase injection process to determine the benefits of injection of gas slugs on acid placement.

APPROACH

A combination of experimental and theoretical work is being carried out to test the efficiency of the gas-assisted acidizing process. In the experiments, we first inject gas into a liquid saturated core until the core is at residual water saturation. We then inject acid until wormhole breakthrough. Acidizing conditions such as temperature, injection rate, nature of fluid saturating the core prior to gas injection, and gas injection method are varied. The permeability response during acidizing is monitored and castings are made of

the wormholes. These results are then compared with the data obtained from experiments on wormholing with liquid alone.

To investigate the efficiency of diversion with gas, we are developing a two-phase acid placement model. This model will incorporate two-phase flow in the reservoir combined with wormhole propagation.

EXPERIMENTAL SETUP

The experiments are conducted using 6” long and 1” diameter cores of Texas Cream. The initial step is to calculate the permeability and porosity of these cores.

An experimental setup has been designed to do the experiments. The setup involves the following basic equipment.

1) A core holder in which the cores are placed. This core holder has a rubber sleeve pressurized at 1500 psi to hold the core firmly so that no annulus remains for the injected fluids to escape without passing through the core. The sleeve is pressurized using an Enerpac pump. A gauge is fitted on the core holder as well as the Enerpac pump to monitor the pressure.
2) A vacuum pump is connected to this core holder so as to evacuate the dry core so that no air remains inside the core before the start of the experiments.
3) A brine tank connected to a pump so as to pump brine to fully saturate the core. A freshwater tank to flush the equipment after the completion of the experiments.
4) Nitrogen gas cylinder to flow nitrogen through the core thereby flushing out all the brine to residual brine saturation and saturating the core with nitrogen gas. This gas cylinder will also be used as a gas supply to the back pressure regulator which is used to maintain a back pressure on the core during the acidizing process to keep CO_2 being liberated dissolved in the solution.
5) Differential pressure transducers to measure the differential pressure across the core during the various injection cycles.

6) A constant volume pump that injects water into an accumulator and displaces acid, which is injected in to the core holder. Thus we are able to control and vary the flow rates of the acid being injected.

7) An electrical oven in which the core holder is placed so as to vary the temperature of experiments. This oven is also used to obtain the Wood's metal castings.

EQUIPMENT AND PROCESS DESCRIPTION

The core is placed inside the core holder. Using the Enerpac pump the pressurized hydraulic oil is injected to the core holder. There are 2 hydraulic oil lines going to the core holder. Firstly the oil is pumped to the end cap. The end cap has a retractable piston head that pushes the core into position. This is necessary, as the coreholder is longer than the core. When the core has been pushed into position, the rubber sleeve is pressurized. The rubber sleeve tightly holds on to the core so that no annulus remains for the liquids to escape without passing through the core. The pressure is monitored using the pressure gauge mounted on the Enerpac pump discharge as well as the pressure gauge mounted on the core holder. Care is maintained so that the pressure doesn't drop below 1500 psi during the experiment.

Now the vacuum pump is started and all the air is evacuated from the tubing and the core. Care is maintained during this process to keep the outlet of the core holder closed.

After all the air has been evacuated, brine is pumped into the core. After pumping brine for a sufficient time period it is assumed that the core is now totally saturated with brine.

Now nitrogen is injected through the core. Until now, no backpressure has been applied on the core. Increasing the gas injection pressure and simultaneously increasing the backpressure on the core outlet slowly brings the core to an outlet pressure of 1000 psi. The gas injection pressure will logically be a little greater (depending on the permeability of the core) than 1000 psi. If needed, a flow meter can be installed in the gas line to measure the amount of nitrogen injected, though this has not been done in the present setup. The N_2 gas is continuously injected and the effluent from the drain of the backpressure regulator is monitored. When it is observed that no more brine is being

produced, it is assumed that residual brine saturation in the core has been achieved and nitrogen injection is stopped.

The final stage is the injection of acid through the core. A constant volume pump is used for pumping a constant volume of water into an accumulator. The accumulator has two chambers separated by a piston. As water is pumped in the bottom chamber it displaces the piston upward thus forcing the acid to flow at the same rate. The pump has a range from 0 to 10 ml/min. When the pumping is started the initial time is measured. The pumped liquid displaces acid and this acid is pumped in to the core. The acid reacts with the core and wormholes are formed. The differential pressure across the core is observed. The inlet and outlet from the core holder are connected to 2 differential pressure transducers. The output data from these two pressure transducers goes to a computer display. In the present setup one pressure transducer has a range of 1200 psi and the other has 2000 psi range.

As the wormhole progresses, the differential pressure across the core drops. Finally when the differential pressure drops to zero the acid has broken thorough. This is the final time. The acid volume pumped is equal to the flow rate multiplied by the difference in initial and final time (in minutes). Using a measuring cylinder we also cross check the pumping rate.

After acidizing has been completed the next process is to make Wood’s metal castings of the wormholes formed by the acid. This is accomplished using an oven. The cores are cased in a PVC pipe and a chunk of Wood’s metal is placed on top of it. Then it is heated in an oven. The Wood’s metal seeps into the core. After this, the core is placed in to a beaker filled with acid. The core is dissolved and the metal castings obtained.

EXPERIMENTAL WORK

We are studying the influence of gas injection on carbonate wormholing in carbonates using the set of experiments shown in Table 1.

Table 1: Experimental Work

Serial	Fluid Saturation	Acid Injection Rate	Temperature	Rock Type and Properties	Wettability	Gas Injection	Status of experiments
A	Brine	Varied from 1 ml/min to 10 ml/min	70° F (Room Temperature)	Texas Cream	Water Wet	No	Completed
B	Brine	Same as set A	70° F (Room Temperature)	Texas Cream; same as Set A	Water Wet	Yes	Completed
C	Brine	Varied from 1 ml/min to 10 ml/min	50 ^{o}C	Texas Cream	Water Wet	No	Completed
D	Brine	Same as Set C	Same as Set C	Texas Cream; same as Set C	Water Wet	Yes	Completed
E	Oil	Varied from 1 ml/min to 10 ml/min	70° F (Room Temperature)	Texas Cream	Water Wet	No	Continuing
F	Oil	Same as Set G	70° F (Room Temperature)	Texas Cream; Same as Set G	Water Wet	Yes	Continuing
G	Brine	Same as Set B	70° F (Room Temperature)	Texas Cream	Water Wet	Inject with acid	Continuing

RESULTS

The primary results of experiments are tabulated below. All the experiments have been performed using water as the initial saturating fluid. The parameters that have been varied are temperature (room temperature or 50 ^{o}C), gas injection (with gas injection or without gas injection), acid injection rates (0.25 ml/min to 10 ml/min).

Table 2: Experimental Results

Expt. No.	Temperature	Initial Saturating Fluid	Gas Injected	Injection Rate (ml/min)	Acid Pore Volumes
1	Room	Water	No	2.7	0.38
2	Room	Water	No	1.0	0.25
3	Room	Water	No	1.5	0.33
4	Room	Water	Yes	2.7	0.38
5	Room	Water	Yes	1.83	0.24
6	Room	Water	No	5.3	0.49
7	Room	Water	Yes	4.12	0.26
8	Room	Water	Yes	2.7	2.8
9	Room	Water	Yes	5.8	0.30
10	Room	Water	Yes	8.0	0.40
12	Room	Water	Yes	1.0	0.16
13	Room	Water	Yes	1.5	0.13
14	Room	Water	Yes	0.5	0.18
15	Room	Water	Yes	0.3	0.20
16	50° C	Water	Yes	4.12	0.21
17	50° C	Water	Yes	5.8	0.20
19	50° C	Water	Yes	1.18	0.28
20	50° C	Water	Yes	0.5	0.45
21	50° C	Water	No	0.5	0.8
23	50° C	Water	No	1.18	0.56
24	50° C	Water	No	1.83	0.31
26	50° C	Water	No	5.8	0.55
28	50° C	Water	No	4.12	0.52
29	50° C	Water	No	1.83	0.44
30	50° C	Water	Yes	1.83	0.28
31	50° C	Water	Yes	2.7	0.25
32	50° C	Water	Yes	1.18	0.32

The volumes of acid injected have been converted to pore volumes to incorporate the variation in the porosity of the cores used for different experiments. The average porosity of the rock from which the cores were taken was 28% and its average permeability was 6.5 mD. The values for each core varied however.

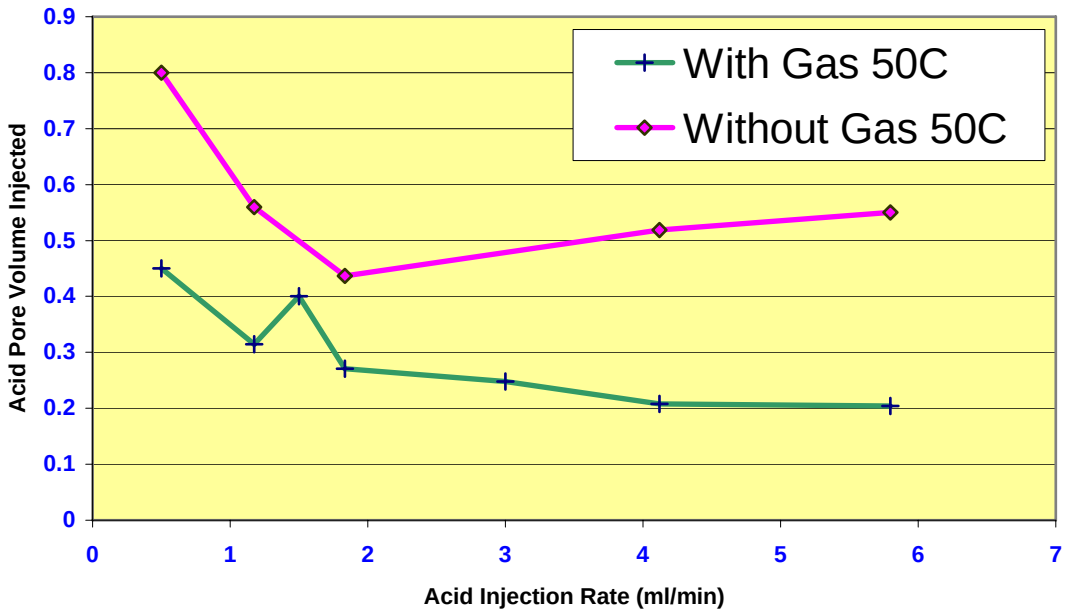

Figure1: Comparison study at 50 ^{o}C

Figure 1 shows a comparison of acid pore volumes required for breakthrough for gas saturated and water saturated cores at temperature of 50 ^{o}C. In the experiments with gas the cores were injected with gas until their water saturation was reduced to residual water saturation and the cores became gas saturated. In the experiments without gas the cores are totally water saturated. It is observed that acid PVTB (pore volumes until breakthrough) required in case of gas saturated cores are 1.5 – 3 times less than those required for water saturated cores.

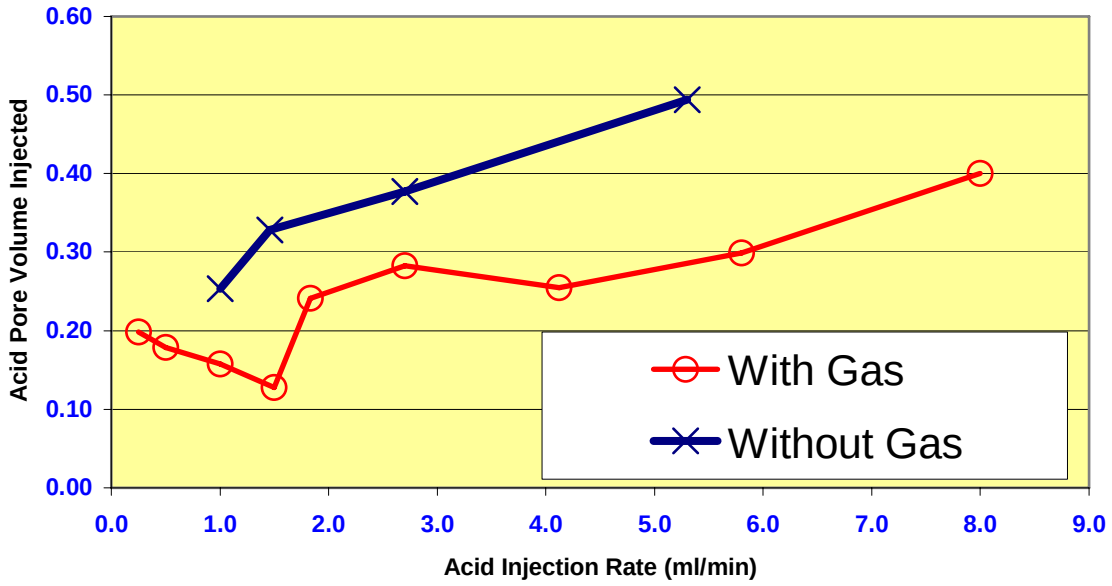

Figure2: Comparison study at room temperature

Figure 2 shows a similar comparison of acid pore volumes required for breakthrough for gas saturated and water saturated cores at room temperature. The acid PVTB (pore volumes till breakthrough) required in the case of gas saturated cores are 1.5 – 3 times less than those required for water saturated cores, just as in the higher temperature experiments.

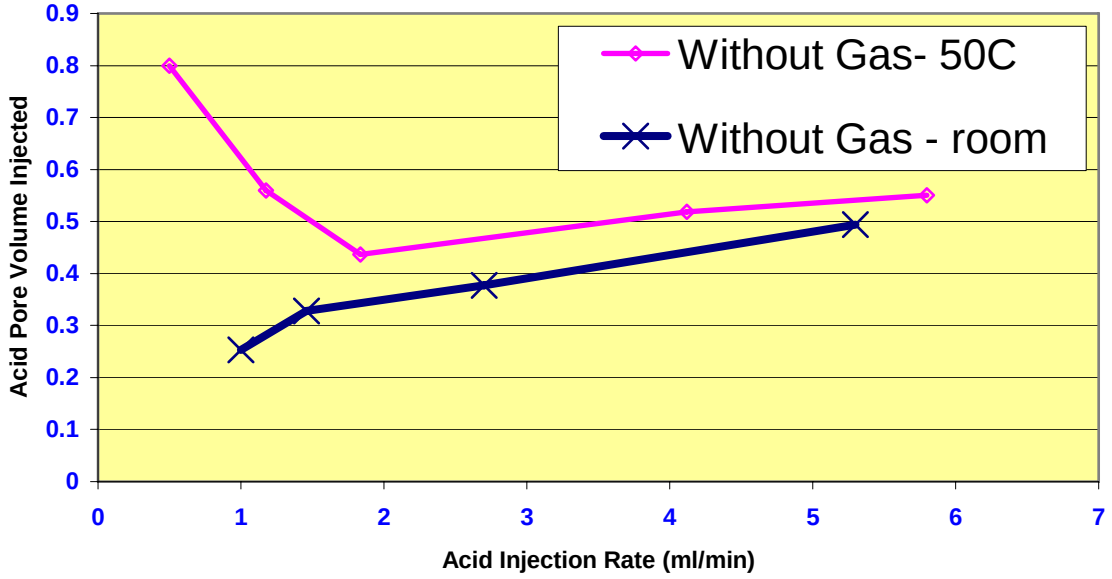

Fig.3: Comparison study of liquid saturated cores at different temperatures

Figure 3 shows a comparison of acid pore volumes required for breakthrough for water saturated cores - at room temperature and at 50 ^{o}C. It was observed that the acid PVTB were lesser at room temperature when compared to those at higher temperature and the optimal rate appears to increase with increasing temperature.

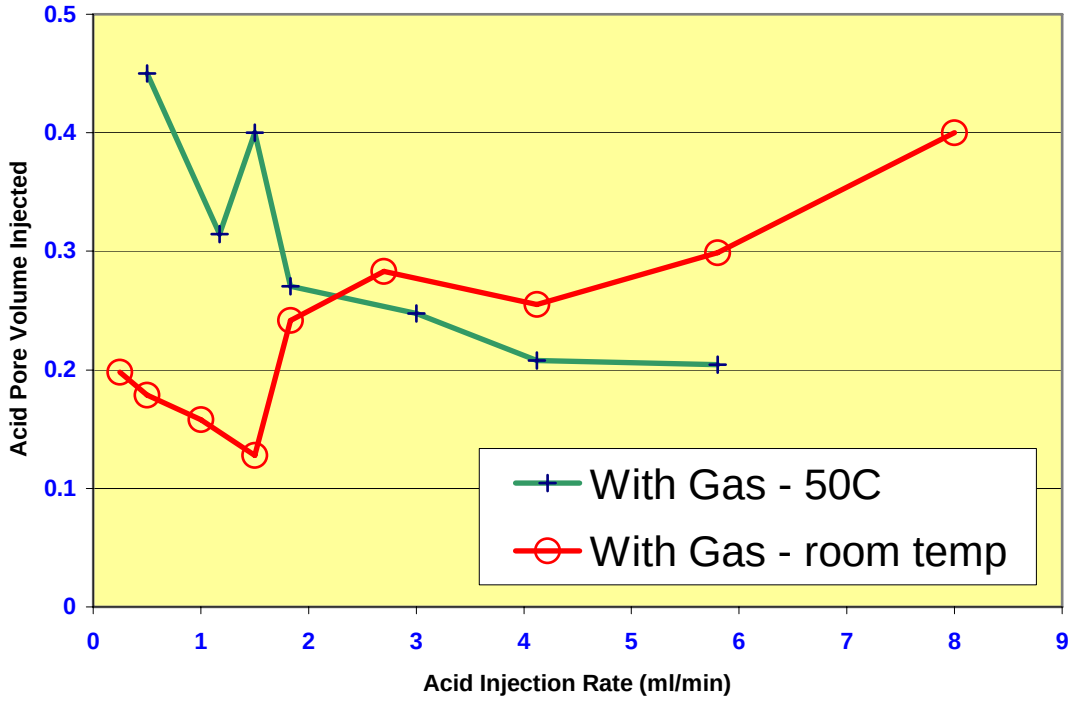

Fig.4: Comparison study of liquid saturated cores at different temperatures

However for gas saturated cores (Figure 4) no definite effect of temperature can be ascertained. At low injection rates, larger acid volumes are needed at higher temperature (similar to the result for liquid saturated cores) but at higher injection rates it is the opposite.

DIRECT COMPARISON OF TWO EXPERIMENTS

Experimental results of Experiments No. 29 and 30 are compared to illustrate our findings. Both Experiments 29 and 30 used similar sized cores, with15% HCl solution at an injection rate of 1.83 ml/ min. Both experiments were performed at 50 ^{o}C temperature. Experiment # 29 was on a water-saturated core with no gas injection. Experiment #30 was a gas-saturated core. The results obtained were quite different. Expt #29 required 0.44 pore volumes (9 mls) of acid for breakthrough. Expt #30 however required acid injection of only 0.28 pore volumes (5.6 mls) to achieve breakthrough.
Figures 5 & 6 show the pressure records for these two experiments. The 0 Pore Volume point is defined as the moment when acid injection into the coreholder begins. Notice that there is a long period of pressure buildup during both experiments, because of compressibility in the system and possibly pump leakage. Once wormholes form the differential pressure begins to decrease and drops very rapidly.

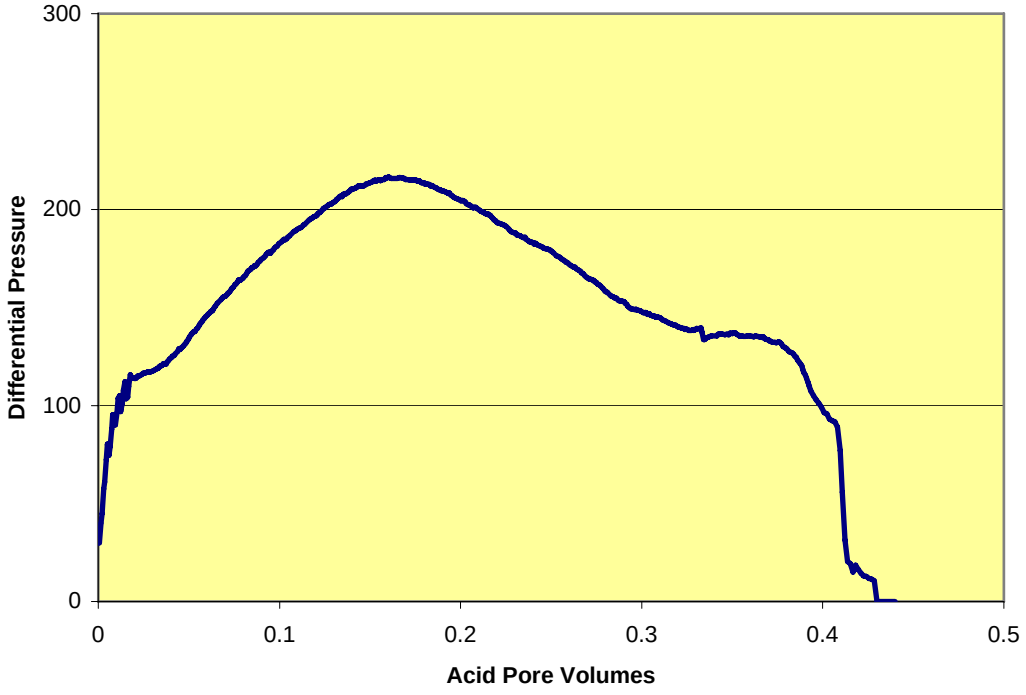

Figure 5: Experiment #29 (Water Saturated Core)

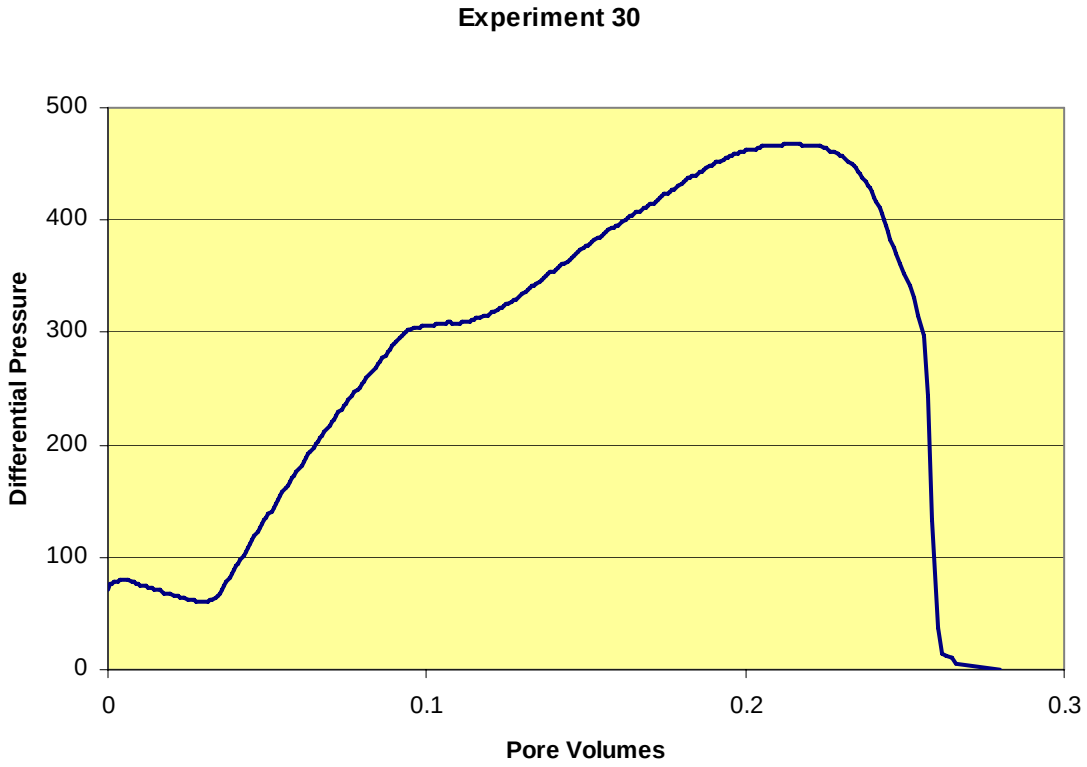

Figure 6: Experiment #30 (Gas Saturated Core)

Figure 7 shows the Wood's metal castings for these experiments. The wormhole made in the gas saturated core was thinner and with less branching indicating that gas saturation reduces fluid leak off thus resulting in more efficient wormholing. The reduced relative permeability to the aqueous phase has reduced the fluid loss from a wormhole propagating through a gas-saturated porous medium.

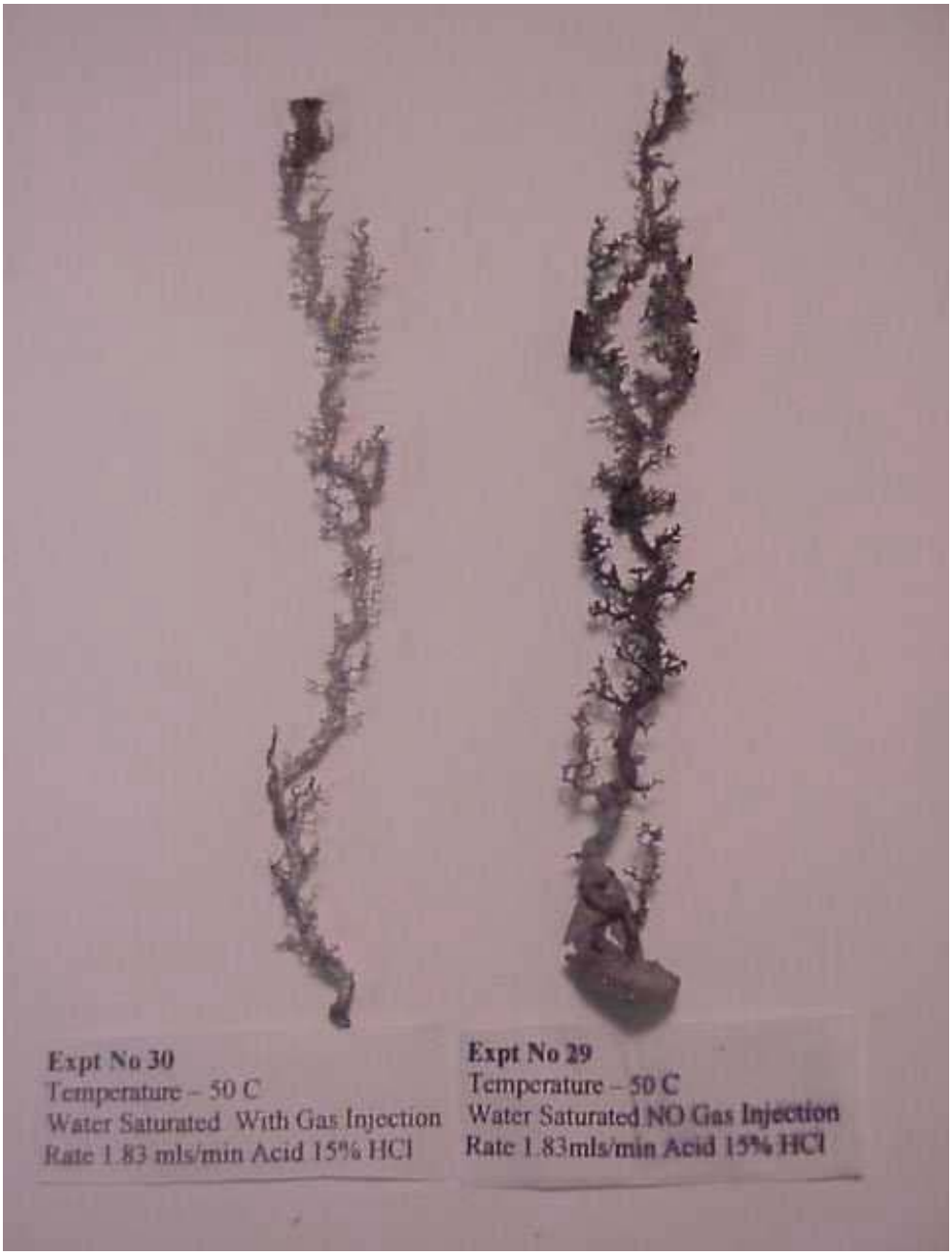

Figure 7: Comparison of Metal Castings

CONCLUSIONS

- The acid PVTB in gas saturated cores are 1.5 to 3 times lesser than that required in liquid saturated cores.
- The PVTB for liquid saturated cores increase with temperature.
- No definite effect of temperature on PVTB was observed in gas saturated cores.

FUTURE SCOPE OF WORK

We have completed the first 4 sets of experiments (A, B, C and D) and plan to complete the rest in this semester. The analysis of these results and the development of a model to predict the wormholing process in an acid/gas system are also continuing.

REFERENCES

1. Wang Y., Hill A.D. and Schechter R.S.: "The Optimum Injection Rate for Matrix Acidizing of Carbonate Formations. " paper SPE 26578 presented at 1993 SPE Annual Technical Conference and Exhibition, Houston, Oct 3-6.

2. Wang Y.: " Existence of an Optimum Rate in Carbonate Acidizing and the Effect of Rock Heterogeneity on Wormhole Patterns." Ph. D. Thesis. University of Texas at Austin (1993)

3. Daccord G., Toubol E., and Lenormand R.: " Carbonate Acidizing: Toward a Quantitative Model of the Wormhole Phenomenon." SPE Production Engineering, February 1989,63-68.

4. Huang T., Hill A.D. and Schechter R. S.: " Reaction Rate and Fluid Loss: The Keys to Wormhole Initiation and Propagation in Carbonate Acidizing" SPEJ, Vol.5, No.3 Sept. 2000, 287-292.

5. Huang T.: "Wormhole Modeling in Carbonate Acidizing" Ph. D. Thesis. University of Texas at Austin (2000)

PROJECT II-2 Development and Validation of a Sandstone Acidizing Permeability Response Model

PRINCIPAL INVESTIGATOR: Dr. A. D. Hill,
RESEARCH SCIENTIST: Dr. D. Zhu
GRADUATE STUDENT: Rasim Serdar Rodoplu

SUMMARY

A large effort has been devoted over the years to modeling of the sandstone acidizing process. Yet, there has been little laboratory validation of the models that are being used. In fact, most comparisons between theoretical models and experiments are still made with just one set of laboratory results - those of Lindsay (1976) conducted with 3 inch Berea cores over twenty years ago. The goal of this project was to develop a rigorous model of the permeability response during sandstone acidizing and to verify this model by comparing it with new laboratory data. This study will be important not only in validation of a permeability model (Panda and Lake, 1994), but also for checking the two-acid, three-mineral model of sandstone acidizing.

Panda and Lake have presented a permeability model which provides a quantitative connection among bulk physical properties of the interconnected pore system (e.g., porosity and tortuosity), the statistics of its particle size distribution (psd) and the effects of cements on the single-phase permeability estimation. Quinn et al. (1994) have used this model as a part of a geochemical simulator of the acidizing process. To apply this model, the reservoir minerals are divided into two groups, detrital grains and diagenic of cements. The diagenic of cement is further sub-divided to pore-filling, pore-lining and pore-bridging. The two-acid, three-mineral model classified the minerals of a typical sandstone as fast-reacting mineral, slow-reacting mineral, and amorphous silica precipitate created as the dissolution process occurs. To apply the permeability model, we define the slow-reacting minerals as detrital and the fast-reacting and precipitating minerals as diagenetic in the permeability model. The permeability model is added to the UTMAST acidizing simulator to make it convenient to perform numerous simulations.

INTRODUCTION TO PERMEABILITY MODELS

Conventional Permeability Model

Up to now empirical correlations relating the permeability increase to the porosity change during acidizing are used. The most common correlations used are those of Labrid (1975), Lund and Fogler (1976), and Lambert (1981). These correlations are:

Labrid:

$$\frac{k}{k_o} = M\left(\frac{\phi}{\phi_o}\right)^n$$

where k_o and ϕ_o are the initial permeability and porosity and k and ϕ are the permeability and porosity after acidizing. M and n are empirical constants, reported to be 1 and 3 for Fontainbleau sandstone.

Lund and Fogler:

$$\frac{k}{k_o} = \exp\left[M\left(\frac{\phi - \phi_o}{\Delta\phi_{\max}}\right)\right]$$

where M= 7.5 and $\Delta\phi_{\max}$ =0.08 best fit data for Phacoides sandstone.

Lambert:

$$\frac{k}{k_o} = \exp\left[45.7\left(\phi - \phi_o\right)\right]$$

Lambert's expression is identical to Lund and Fogler's when M / $\Delta\phi_{\max}$ = 45.7

Using the values of the constants suggested, Labrid's correlation predicts the smallest permeability increase, followed by Lambert's, then Lund and Fogler's. The best approach in using these correlations is to select the empirical constants based on core flood responses, if such are available. Lacking data for a particular formation, Labrid's equation will yield the most conservative design [Economides et al. (1994)].

The models presented above predict permeability changes by changes in porosity based on empirical parameters, and ignored the impact of the particle size distribution (psd) or cement content on the permeability estimate. Thus, the models yield extremely inconsistent results.

Permeability Mode with Mineralogy Effect

In 1995 Lake and Panda developed a permeability model to quantify the effects of cements on the single-phase permeability estimate of a consolidated medium. Their original work was based on a permeability model developed by Kozeny (1927) and Carman (1937). We have discussed the model development in our last report. The equation to calculate permeability response presented by Panda and Lake is expressed as

$$k = \frac{\overline{D}_p{}^2 \phi^3 \left(\gamma C_{Dp}{}^3 + 3C_{Dp}{}^2 + 1\right)^2}{2\tau_e (1-\phi)^2 \left[6\left(1 + C_{Dp}{}^2\right)(1-\phi_u)/(1-\phi) + (a_{vb}P_b + a_{vl}P_l + a_{vf}P_f)\left(\gamma C_{Dp}{}^3 + 3C_{Dp}{}^2 + 1\right)\right]^2} \tag{1}$$

where

D_p = Mean particle diameter (L)

γ = Skewness of a psd

C_{Dp} = Coefficient of variation = standard deviation/mean

α_v = Specific surface area (L^{-1})

P_b,P_l,P_f= Amount of pore-bridging,pore-lining, and pore-filling cements,fraction

τ_e = Effective tortuosity which is given by:

$$\tau_e = \tau_u \left(1 + C_{Dp}{}^2\right)\left(\frac{1}{1-m_1}\right)^2 \left[1 + \frac{m}{(1-m)(\phi_u)^{0.33}}\right]^2 \tag{2}$$

m,m_1= fractional pore-filling and pore-bridging cement content (as a fraction of the unconsolidated pore volume)

$$m = \frac{(1-\phi)}{\phi_u} P_f \qquad m_1 = \frac{(1+\phi)}{\phi_u} P_b \tag{3}$$

The model gives a more complete representation of the flow conductivity of a consolidated permeable medium because it uses all the relevant permeable medium

properties such as porosity, tortuosity, cement composition, and statistic properties of the rock.

ANALYSIS OF PARAMETERS

Tortuosity

Many attempts have been made to improve Kozeny's equation to make it model flow better in real porous media. One improvement is to recognize that the bundle of capillary tubes are tortuos, so that the effective flow length through any tube, L_e, is greater than the bulk length of the porous medium, see Fig. 1.

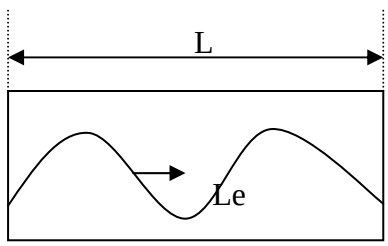

Tortuosity = $(L_e / L)^2$

L_e: Effective flow length through any tube

L : Bulk length of porous medium

Fig. 1 Schematic of tortuosity.

In the model, the effective tortuosity is related to cement effect by Eqs. 2 and 3. So, a change in cement content affects directly the reservoir tortuosity.

Coefficient of Variation

The coefficient of variation (C_{dp}) of the particle size distribution is used to describe the amount of variation in the population. Fig. 2 shows the permeability response predicted by the new model when C_{dp} changes from 0 to 1. From literature data as summarized in Table 1 (Winsauer et al., 1952 and Folk, 1965), this range is more than the usual C_{dp} range.

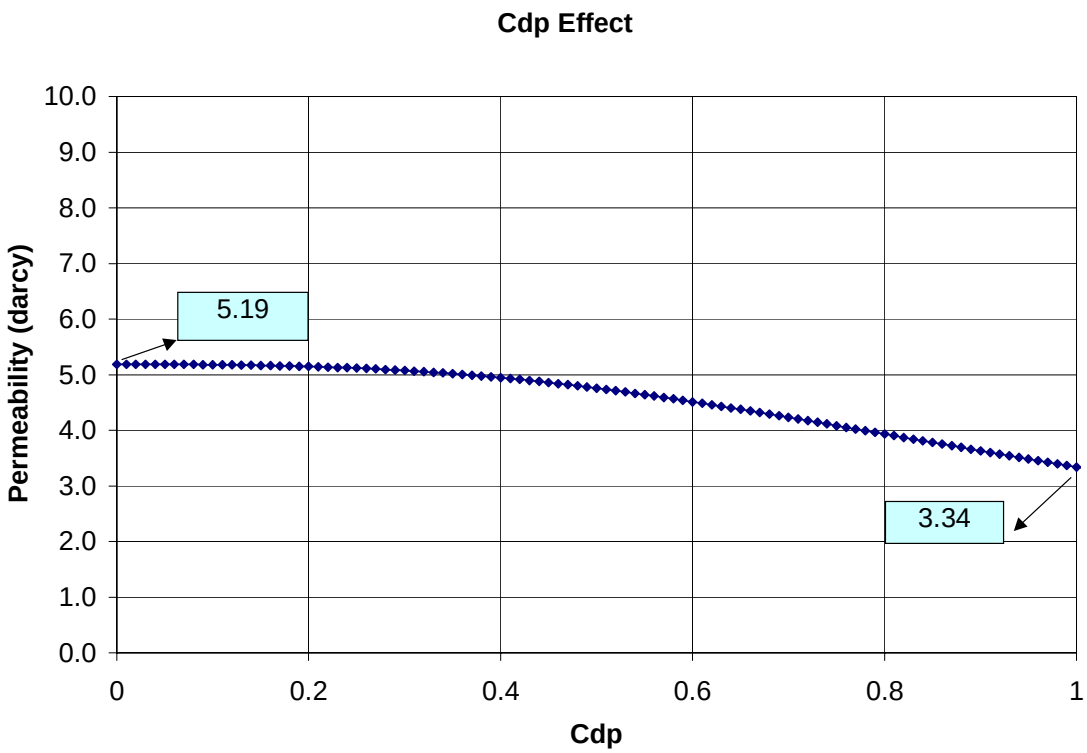

Fig. 2 Permeability response to changing coefficient of variance.

Table 1. Common values of particle size distribution parameters

Standard Deviation	
Very Well Sorted	under 0.35
Well Sorted	0.35 to 0.50
Moderately Well Sorted	0.50 to 0.71
Moderately Sorted	0.71 to 1.00
Poorly Sorted	1.00 to 2.00
Very Poorly Sorted	2.00 to 4.00
Extremely Poorly Sorted	over 4.00
Skewness	
Strongly Fine Skewed	+1.00 to +0.30
Fine Skewed	+0.30 to + 0.10
Near Symmetrical	+0.10 to -0.10
Coarse Skewed	-0.10 to -0.30
Strongly Coarse Skewed	-0.30 to -1.00
Tortuosity	
Unconsolidated Sandstone	1.4
Consolidated Sandstone	1.5 - 3.3

Winsauer et al. (1952) and Folk (1965)

Skewness

Skewness is a measure of the degree of a symmetry of a distribution. In other words we can define skewness as a measure of the asymmetry of the data around the sample mean. If skewness is negative, the data are spread out more to the left of the mean than to the right. Fig. 2 illustrates the basic definition of skewness. If skewness is positive, the data are spread out more to the right. The skewness of the normal distribution (or any perfectly symmetric distribution) is zero.

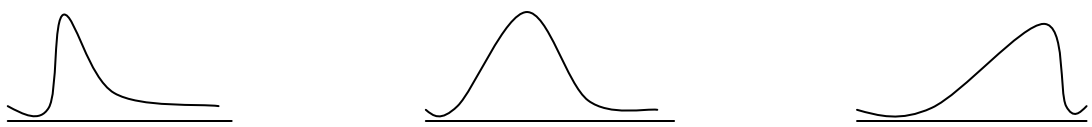

$\lambda > 0$ $\lambda = 0$ $\lambda < 0$

(Negatively skewed PDF) (Symmetrical PDF) (Positively skewed PDF)

Fig. 2 Illustration of Skewness.

The model prediction of permeability change with skewness when other parameters are constant can be seen in Fig. 3. The cement content effect on permeability can be seen in Fig. 4. Please note that for skewness or coefficient of variation, permeability changes approximately from 3.5 md to 5 md while we observe much more increase up to 250 md by dissolving cementing minerals. Comparing cement content effect on particle size distribution parameters such as skewness and coefficient of variation, we observed that

1. The most important parameter that is considered by the model is the amount of cementing materials.
2. Particle size distribution parameters can be taken as constant.
3. Tortuosity change is already being considered by change in cement content.

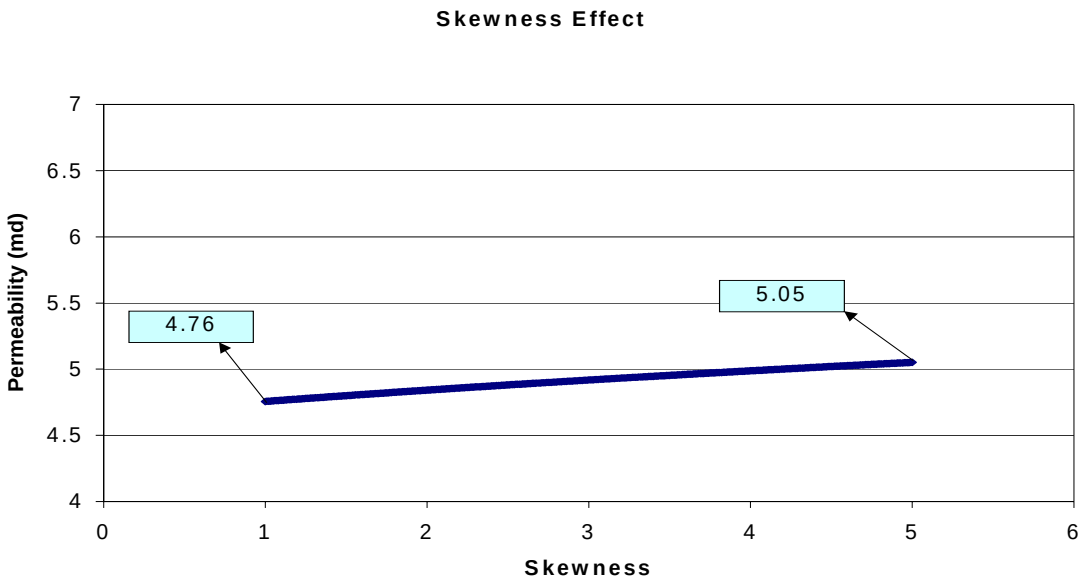

Fig. 3 Effect of skewness on permeability predicted by the new model.

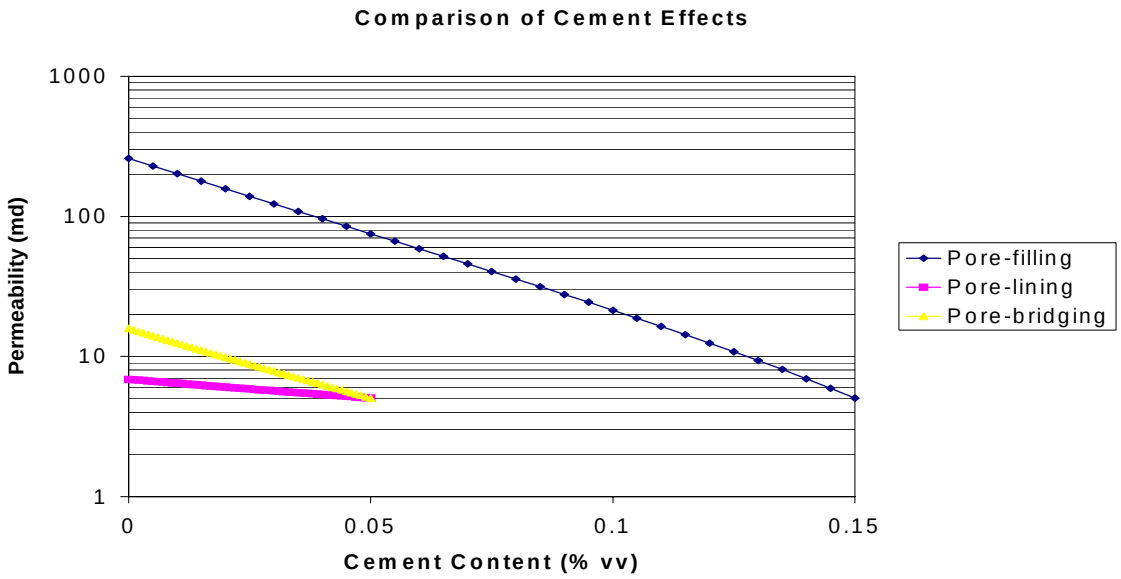

Fig. 4 Effect of cement content on permeability predicted by the new model.

Since the most important parameter in the model is cement content, let us expand on these cementing materials and some of their properties that causes significant change in permeability during acidizing process.

The model represents pore-filling, pore-lining, and pore-bridging cements by treating the cement particles as rectangular crystals attached radially to detrital grains. The classification of dispersed clays is proposed by Neashman (1977).

1- Pore-filling (Discrete particle) clays reflect the typical mode of occurrence of kaolinite in sandstones. It usually develops as pseudohexagonal, platy crystals attached as discrete particles to pore walls or occupying intergranular pores (Fig. 5a).

2- Pore-lining clays are attached to pore walls to form relatively continuous and thin clay mineral coating (Fig. 5b). Illite, chlorite, and montmorillonite clays have been observed with pore lining crystal morphologies.

3- Pore-bridging clays in addition to being attached to pore wall surfaces extend far into or completely across a pore or pore throat to create a bridging effect (Fig. 5c). These include illite, smectite and montmorillonite varieties.

These three categories are described for hydrocarbon-bearing sandstones using scanning electron microscopy and correlated to rock geological-petrophysical parameters commonly used in reservoir evaluation. The characteristics of the major types of dispersed clays are summarized in Table 2.

We are also implementing the Panda and Lake's permeability model into our acidizing simulator, UTMAST, to replace the Labird model we used before. In the following Fig. 6 we see the comparison of permeability responses predicted by the new permeability model and Labrid's model which is currently used in UTMAST acidizing simulator. As acid injected and minerals dissolve after a certain amount, permability levels off and gives very slight change in Labrid's model, on the other hand new model predicts continuos increase but with a decreasing slope.

EXPERIMENTAL VERIFICATION OF SANDSTONE ACIDIZING MODELS

We developed a plan for a series of coreflood experiments aimed at testing the two-acid, three-mineral model of sandstone acidizing and the new model of permeability change during acidizing. The experimental study is being conducted at the acidizing research lab of the Langfang Research Branch of CNPC, China.

Table 3 below summarizes the experiments that are planned. In these experiments, we will vary mineralogy, injection rate, temperature, and preflush and main acid stage concentrations. Tests will be conducted at 25 °C and 75 °C and at 4 different injection rates. The experiments can be divided into 5 groups. The first four groups of experiments are for different temperatures and injection rates, and in the last set we will change the preflush concentration to 5% HCL. We will monitor the permeability change to determine the total volume of HF/HCl mixture to inject. The core permeability will be continuously monitored during each experiment.

The sandstone samples used in the study are Antolini, Antelope, and Berea sandstone. The Antolini and Antelope sandstones are relatively high permeability Aeolian sandstones (permeabilities raged from 40 - 1100 md), obtained from outcrops in Arizona. The mineralogy of these samples are being measured at the laboratory in Langfang. The contrast of the rock properties will provide a wider range of data for different sandstone to verify the permeability response model.

CONCLUSIONS

In this project, by using new experimental data with a rigorous permeability response model, the uncertainty in predicting permeability will be avoided. This model relates the permeability of a permeable medium to the porosity, particle size distribution statistics, and the amount of various cementing minerals present.

FIGURE Ia. - "DISCRETE PARTICLE" KAOLINITE

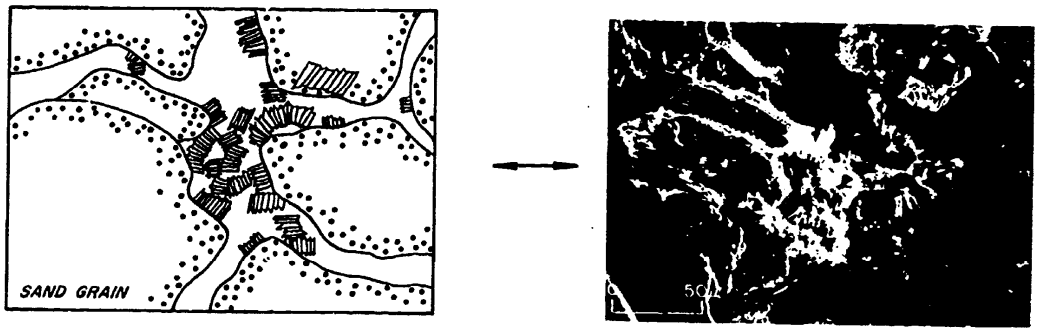

FIGURE Ib. - "PORE-LINING" CHLORITE

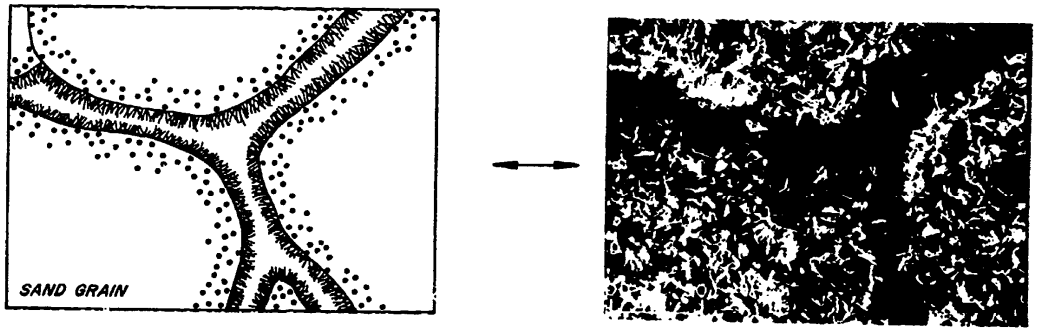

FIGURE Ic. - "PORE-BRIDGING" ILLITE

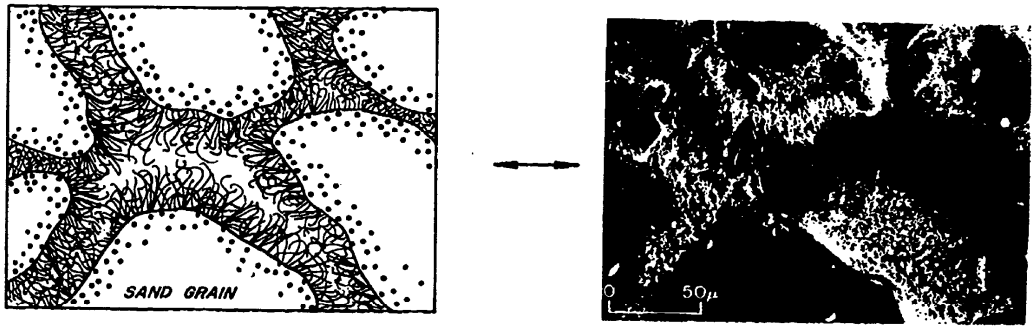

Fig. 1 - Three general types of dispersed clay in sandstone reservoir rock.

Fig. 5 Classification of cementing materials

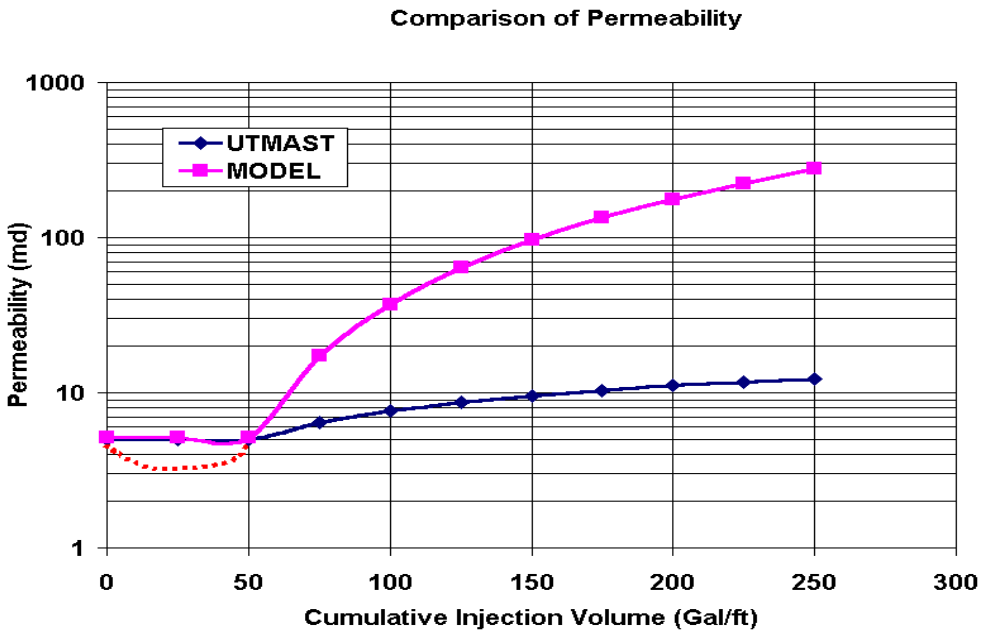

Fig. 6 Permeability calculated from different model.

Table 2. Properties of a Few Commonly Occurring Cements

Cement	Type	Cement Cluster Shape Assumed	Length (μm)	Width (μm)	Specific surface Area (per mm)
Smectite	Bridging	Rectangular	10-50	5-20	240-1533
Chlorite	Lining	Semicylindrical (rosette-shaped clustering)	5-20	20-150	127-600
Kaolinite	Filling	Semicylindrical (book-shaped clustering)	150-2500	2-20	100-1000
Calcite	Filling	Cubic	30-50	-	120-200
Dolomite	Filling	Cubic	10-50	-	120-600
Quartz/Pyrite	Filling	Rectangular	30-100	20-80	85-300
Siderite	Filling	Rectangular	10-50	5-25	200-1000
Illite	Bridging	Rectangular	-	-	-

4. Warner (1964), Stalder (1973), Neasham(1977), Pallat et all. (1984), Nadeau (1985)

Experiment No	Preflush	Main Acid Treatment	Temperature (^{0}C)	Injection Rate (ml/min)
1	15 % HCL	9%HCL, 1%HF	25	3.5
2	"	9%HCL, 1%HF	25	10
3	"	9%HCL, 1%HF	25	15
4	"	9%HCL, 1%HF	25	20
5	"	9%HCL, 1%HF	75	3.5
6	"	9%HCL, 1%HF	75	10
7	"	9%HCL, 1%HF	75	15
8	"	9%HCL, 1%HF	75	20
9	"	12%HCL, 3%HF	25	3.5
10	"	12%HCL, 3%HF	25	10
11	"	12%HCL, 3%HF	25	15
12	"	12%HCL, 3%HF	25	20
13	"	12%HCL, 3%HF	75	3.5
14	"	12%HCL, 3%HF	75	10
15	"	12%HCL, 3%HF	75	15
16	"	12%HCL, 3%HF	75	20
17	5% HCL	12%HCL, 3%HF	25	10
18	5% HCL	9%HCL, 1%HF	25	10

NOMENCLATURE

a_v	=	Specific surface area (L^{-1})
a_{ve}	=	Effective specific surface area (L^{-1})
C_{Dp}	=	Coefficient of variation = standard deviation/mean
D_p	=	Diameter of particle (L)
$\overline{D_p}$	=	Mean particle diameter (L)
k	=	permeability (L^2)
m	=	Amount of pore-lining, fraction of original pore volume
m_1	=	Amount of pore bridging cement, fraction of original pore volume
psd	=	Particle size distribution
P_b,P_l,P_f	=	Amount of pore-bridging, pore-lining, and pore-filling cements,fraction of the total solid volume
V_b	=	Bulk volume of the permeable medium
ϕ	=	Bulk connected porosity
ϕ_u	=	Porosity of an unconsolidated sand
γ	=	Skewness of a psd
σ	=	Standard deviation of a psd
τ_l	=	Tortuosity caused by pore-lining cement
τ_e	=	Effective tortuosity
τ_u	=	Effective tortuosity of an unconsolidated sand of single-size particles

REFERENCES

Economides, M. J.; Hill A. D.; Ehlig- Economides, C.: Petroleum Production Systems, Prentice-Hall, Englewood Cliffs, NJ,1994.

Lindsay, D.M. An Experimental Study of Sandstone Acidization, Report No. UT 76-1, Texas Petroleum Research Committee, The University of Texas at Austin, Austin, Texas, 1976.

Neashman, J. W. The Morphology of Dispersed Clay in Sandstone Reservoirs and Its Effect on Sandstone Shaliness, Pore Space, and Fluid Properties. SPE 06858 presented at the Annual Technical Conference and Exhibition of the SPE of AIME, Denver, CO, 1977.

Panda M.N., and L.W. Lake, Estimation of Single-Phase Permeability from Parameters of Particle Size Distribution: AAPG Bulletin, v. 78, no.7, p.1028-1039, 1994.

Panda M.N., and L.W. Lake, A Physical Model of Cementation and Its Effects on Single-Phase Permeability: AAPG Bulletin, v. 79, no.3, p.431-443, 1995.

Quinn, A., Designing Effective Sandstone Acidizing Treatments Through Geochemical Modeling: MS. Thesis, University of Texas at Austin, Austin Texas, 1994.

PROJECT TITLE: II-3 **MATRIX ACIDIZING OF NATURALLY FRACTURED CARBONATE RESERVOIRS**

PRINCIPAL INVESTIGATOR: **DR. A. D. HILL**

RESEARCH SCIENTIST: **DR. D. ZHU**

GRADUATE STUDENT: **DR. CHENGLI DONG**

Summary

The original purpose of this project is to develop a mathematical model to simulate acid penetration in naturally fractured carbonate reservoirs, and to predict stimulation results of the wells in carbonate formations.

In IWP Phase I, we started with lab experiments of acidizing carbonates containing fractures to observe the etching patterns of acid flow in carbonate fractures.. The result shows that acidizing fractured carbonates results in three etching patterns in fractures: channels, wormholes and surface etching, which depend on the fracture width and the surface roughness. At the lab-scale acidizing experiments, leakoff acid has little effect on etching patterns. Based on our experimental results, a mathematical model was developed. Rough-surfaced fractures were numerically generated and implemented in the simulator based on the model. The simulator predicts the same acid etching patterns and the same relations between acid etching patterns and fracture properties observed in experiments.

In IWP Phase II, we first developed a parallel computing version and the computation speed is largely increased. Large single fractures (0.6 cm by 0.06 m) were implemented in the simulator and the results show that when the fracture width is on the order of 10^{-3}cm, wormholes will always be created when far enough away from the inlet side. Increasing leakoff reduces the acid penetration distance and makes the channel broader.

In the simulations of acidizing two intersected fractures, we found that at the intersection point of two fractures, acid tends to flow through and create wormholes in only one fracture even if they all have the same properties. When the two fractures have different properties, acid tends to flow and etch through the fractures with larger hydraulic width or rougher surfaces. By reviewing the literature on the topic of properties

of the natural fracture network, we found that only a small fraction of the fractures in the network form the backbone that provides the main flow path for acid flow. The length distribution in the main flow path (backbone) obeys the power law as in the entire network. In simulations of acidizing fracture networks, acid flows and etches along the main flow path. When acid is injected with a high rate, usually the entire surfaces of the first several fracture in the main flow path are etched by acid and form a very broad channel. This trend may be stopped by an initially small width fracture that becomes a barrier. The channel usually stops propagation before an initially small width fracture.

The model was finally applied to some typical field conditions. The overall acid penetration distance predicted by the model is usually longer than the acid penetration distance in a matrix rock without fractures. We used Prats's skin factor model to calculate skin factor after acidizing. The result shows that the skin factor from acid stimulation of a well in a naturally fractured reservoir can be -2 to –3, which is often observed in the field.

We have implemented the model to a computer software, UTAcidFrac. The calculation was coded by C++, and the interface was in JAVA.

The publications from this project include:

1. Dong, C., Hill, A. D. and Zhu, D.: "Acid Etching Patterns in Naturally-Fractured Formations," SPE 56531, presented at the SPE Technical Conference and Exhibition, Houston, Oct. 4-6, 1999.
2. Dong, C.: "Acid Etching Pattern in Naturally-Fractured Carbonate Reservoirs," M.S. Thesis, the University of Texas at Austin, TX, December 1999.
3. Dong, C., Zhu, D. and Hill, A. D.: "Modeling of the Acidizing Process in Naturally-Fractured Carbonates," SPE 63183, presented at the SPE Technical Conference and Exhibition, Dallas, Oct. 2-4, 2000.
4. Dong, C., Zhu, D. and Hill, A. D.: "Acid Penetration in Natural Fracture Networks," SPE 68927, presented at the SPE European Formation Damage Conference held in The Hague, The Netherlands, 21–22 May 2001.
5. Dong, C.: "Acidizing of Naturally-Fractured Carbonate Formations," PhD. Dissertation, the University of Texas at Austin, TX, August 2001.
6. A. D. Hill, D. Zhu, C. Dong, and A. Luna Garcia: "Matrix Acidizing of Naturally

Fractured Carbonate Formations," *JPT* 56531, presented at the SPE Technical Conference and Exhibition, Houston, Oct. 4-6, 1999.

7. Dong, C., Hill, A. D. and Zhu, D.: "Acidizing in Naturally Fractured Carbonate Reservoirs," SPE 75252, will be presented at the SPE/DOE Thirteenth Symposium on Improved Oil Recovery held in Tulsa, Oklahoma, 13–17 April 2002.

We also developed a software based on the model from this project. The simulation model was coded by C++, and the interface was generated by JAVA.

PROJECT TITLE, #II-4 Field Application of Simulator for Foam-Acid Diversion

PRINCIPAL INVESTIGATOR: Bill Rossen

GRADUATE STUDENT: Liang Cheng

SUMMARY

This project issued one SPE manuscript and one Ph.D. dissertation this year:

Cheng, L., Kam, S. I., Delshad, M., and Rossen, W. R.: "Simulation of Dynamic Foam-Acid Diversion Processes," SPE 68916 presented at the 2001 SPE European Formation Damage Symposium, The Hague, 21-22 May.

Cheng, L.: "Simulation Studies of Foam-Acid Diversion," Ph.D. dissertation, The University of Texas at Austin, 2002.

Both are included on the CD-ROM that includes this report.

The SPE paper summarizes our recent work on developing, validating, and applying a simulator for foam-acid diversion. The SPE manuscript is substantially similar to chapter 4 of Liang Cheng's Ph.D. dissertation. The dissertation chapter also includes a few checks and modifications made after completion of the manuscript, however. Therefore, the conclusions below are taken from the dissertation chapter:

1. A simulator for foam-acid diversion (chemical-flood simulator UTCHEM, modified for foam) is described, that for the first time explicitly accounts for the effects of gas trapping on liquid mobility and the effect of pressure gradient on gas trapping. With this simulator one can account for effects of gas saturation and compressibility on foam-acid diversion processes. An algorithm for fitting the parameters of the model to steady-state laboratory data is presented in both the dissertation and the SPE manuscript. A sample UTCHEM input file is included in the dissertation.
2. The foam model in the simulator fits steady-state foam mobility in both high- and low-quality flow regimes, and the apparent non-Newtonian rheology of liquid injected after foam.
3. The simulator qualitatively fits the transition period observed between steady-state foam and liquid injection in laboratory corefloods. It correctly predicts the

effects of gas compressibility and a shut-in period on this transition and on steady-state liquid mobility after foam. The dynamics of this transition are complex. For instance, at the start of liquid injection, most of the core briefly experiences a burst of drier gas flow, as pressure gradient decreases and gas already in the core expands.

4. A foam generator and associated tubing and fittings upstream of the core inmost previous coreflood studies acts as a "dead volume" during liquid injection that can significantly affect the results and especially the transition period. Simulations suggest that this dead volume is the cause of th simultaneous decline in pressure gradient in all sections of the core observed in previous studies.
5. Applied to radial flow, the simulator suggests that the transition period between foam and liquid injection may not last as long or be as significant in field application as in laboratory corefloods. In the cases studied, the transition between steady states is largely over within about 15 to 30 minutes.
6. The fit of the simulator to laboratory data is not quantitative. In most cases the simulator fit to steady-state data predicts a faster transition period than observed in the experiments. This casts some doubt on conclusion 4. Further study is needed.

Liang Cheng spent much of the remainder of 2001 verifying the accuracy of the numerical routines in simulator UTCHEM as applied to foam. This work is summarized in chapter 2 of his dissertation. The conclusions of this chapter are as follows:

1. A foam simulator based on the "fixed-P_c*" model has been implemented into the UTCHEM reservoir simulator. It can describe foam flow in both low- and high-quality regimes, as well as the shear-thinning behavior in low-quality regime.
2. Effects of foam model parameters on foam behavior are examined, and a procedure for fitting the foam model parameters to foam data is described in the dissertation.
3. Comparison between simulation and fractional-flow methods for the same foam-injection and post-foam liquid-injection processes has validated the foam simulator, and revealed two numerical artifacts: fluctuations of water saturation ahead of foam front, and a small delay in foam propagation.
4. Two models of the dependence of foam strength on surfactant concentration are studied. Making foam generation a nonlinear function of surfactant concentration can artificially accelerate foam propagation; making foam suddenly appear at a

threshold concentration can artificially slow foam propagation. Both artifacts depend on numerical or physical dispersion. Both artifacts could be more severe in simulations using fewer grid blocks or less rigorous control of numerical dispersion than in UTCHEM. Simulation practitioners should check the extent of numerical dispersion of surfactant concentration and its effect on foam propagation. The results confirm Zeilinger's (Ph.D. dissertation, The University of Texas at Austin, 1996) finding that, in the absence of dispersion, the foam front propagates as an indifferent wave, i.e., a shock front, with velocity independent of how foam strength depends on surfactant concentration.

Interested readers are referred to these two documents for further details.

II-5. Cleanup of Wall Building Filter Cakes and Perforations during Flowback

Rana S. Roy, Mukul M. Sharma

Project Summary

Details of the project are presented in Rana S. Roy's M.S. thesis. A summary of the main accomplishments of the project is presented below.

Studies conducted earlier indicate the importance of solids invasion on determining the magnitude of Flow Initiation Pressure (FIP). Other studies have shown that relative permeability effects can play an important role in determining the FIP. In this study we clearly identify the conditions under which solids invasion and relative permeability effects can play important roles.

Experiments are conducted with brine saturated cores and cores containing a residual brine saturation. FIP measured by flowing back with brine and with oil are reported. It is shown that for high permeability rocks (k>200 md) the FIP is determined largely by the internal filter cake formed by solids invasion. Surprisingly the external cake contributes very little. However, in cases where the filtrate leak-off is large, relative permeability effects can become increasingly important. A key difference between these two components of FIP is that while relative permeability effects will dissipate with time, internal filter cakes may not.

A quantitative model to calculate the FIP is presented which allows us to evaluate the relative magnitude of the pressure drop caused by relative permeability effects versus that caused by solids invasion. The results of this study clearly show that both solids invasion and filtrate invasion can play an important role in determining the FIP. In addition factors such as the relative mobility of water and oil and the depth of invasion of solids are important parameters. A method is presented that allows us to estimate FIP values in the field based on static filtration tests conducted on cores.

II-6. Sizing Solids in Drilling and Completion Fluids

Ajay Suri and Mukul M. Sharma

Project Summary

Details of the project are presented in Ajay Suri's M.S. thesis. A summary of the main accomplishments of the project is presented below.

One of the most effective ways of preventing formation damage to the reservoir during drilling and completion operations is the formation of internal and external filter cakes which form an ultra-low permeability barrier between the wellbore and the reservoir rock. This strategy is used to control fluid loss (from the wellbore to the formation) during drilling, completion and stimulation operations. It is generally expected that when the well is put back on production this wall building material will degrade or be produced back due to the pressure drawdown. In practice, however, it is quite commonly observed that a very small fraction of the wall building material is removed while most of the wellbore, fracture or perforation still remains blocked by the filter cake so that only a small portion of the flow area contributes to the inflow of oil. This is primarily because once a small fraction of the wellbore (or one or two perforations) are open to flow there isn't sufficient pressure gradient to remove the wall building material from the other perforations or from the other parts of the formation face.

Over the past two years we have conducted experiments to evaluate the formation damage and flowback properties of the filter cakes formed by sized calcium carbonate, sized salt and bentonite muds. The rock permeability, the overbalance pressure, the flowback rate and the particle content of the muds all play an important role in determining the pressure gradient needed to remove the cake. It was shown that the flowback pressure is controlled primarily by the internal filter cake and the extent of filtrate invasion. Conditions for cake liftoff and pinhole formation in cakes were not clearly established.

A model has been developed to estimate the depth and degree of formation damage caused by mud particles present in drilling or completion fluids. The mud components are characterized as particles with different sizes. The depth of damage and permeability loss

is calculated after invasion of the mud and also after flowback. The effect of the particle size distribution in the fluid, particle concentration, differential pressure across the core, and permeability of the formation are studied. It is demonstrated that particle invasion and flowback processes are largely dependent on the particle size in the mud and the permeability of the formation. The results of the model are shown to agree well with mud filtration experiments.

It is shown that bridging materials in the mud need to satisfy two criteria: (1) They should not penetrate the reservoir rock pores to induce damage, and (2) they should act as good filtration control agents for the other colloidal material such as polymers in the mud. Past work has not adequately recognized the importance of the second sizing criteria. Experiments and models conducted over the past two years clearly show that in many instances the damage is primarily caused by our inability to prevent the invasion of polymers and other fine-grained solid additives into the formation.

To better estimate the particle size distribution in drill-in and completion fluids, different methods for measuring particle sizes were investigated. These results show that the measured particle sizes can vary over two orders of magnitude depending on the technique used and on sample preparation. Based on a comparative analysis of several samples, light scattering techniques are recommended for measuring the particle size distribution. Recommendations for sample preparation are also provided.

Based on the model and our ability to measure particle size distributions, fluids can be designed and formulated to minimize solids invasion and maximize return permeability.

Improved Well Performance Research Program

Project # II-7

Modeling Multiple Hydraulic Fractures in a Naturally Fractured Reservoir

Shashank Raizada, MS

The University of Texas at Austin, 2002

Supervisor: Jon E Olson

OBJECTIVE

Our objective is the study hydraulic fracturing in naturally fractured reservoirs, with emphasis on fracture propagation and branching, multiple fracturing, and fluid leakoff. We will formulate a Pseudo-3d code that will explicitly incorporate the interaction of multiple simultaneously propagating fractures, accounting for fracture branching and non-planar propagation.

INTRODUCTION

Natural fractures can affect hydraulic fracturing operations by greatly increasing fluid leakoff, causing variations in the stress near the wellbore and by altering the path of hydraulic fracture propagation. This can lead to near wellbore tortuosity, multiple hydraulic fractures and reduction in fracture width, resulting in higher net pressures, shorter fractures and the possibility of a premature screen out (Warpinski and Teufel, 1987; Cleary et al., 1993; Hossain et al., 2000). Most commercially available models simulate a single planar fracture propagating in a laterally homogeneous formation. The presence of natural fractures may be treated in a continuum sense by altering fluid leak-off, in particular including pressure sensitive effects. However, none can explicitly model the interaction between multiple fractures in the vicinity of the wellbore nor at a distance.

MULTI-STRANDED HYDRAULIC FRACTURES

Multi-stranded hydraulic fractures are those that grow simultaneously from a wellbore and penetrate far into the formation during fracturing. Multiple fractures can initiate at the wellbore due to perforation effects or the presence of natural or drilling induced fractures intersecting the wellbore. However, it is typically assumed that only

one fracture propagates beyond this near-wellbore area. The other fractures are assumed to either coalesce in the near-wellbore area or cease growth due to the stress influence from other nearby fractures. Fast et al. (1992) and Warpinski et al. (1991) have shown that this "single far-field fracture" assumption can be wrong, and that multiple hydraulic fractures often continue growing in the far-field region. Evidence from coring through propped hydraulic fracture treatments in reservoirs has confirmed the simultaneous growth of multiple hydraulic fractures. In one 4-feet core, 30 fractures were found over 60 ft away from the point of fracture initiation.

Two possible growth patterns have been postulated for multi-stranded hydraulic fracture (Figure 1):

1. Fractures grow more or less independently of each other along different parts of the wellbore or in different layers (Elbel et al., 1992); or
2. Fractures grow parallel to each other and compete for fracture opening space (Warpinski and Teufel, 1987).

The propagation of independent multiple fractures may occur when multiple perforated intervals are treated, or when the lateral separation between fractures is large compared to the fracture height (e.g. in deviated wells). These multiple fractures may propagate as individual strands or may interfere with each other. The presence of natural fractures leads to more complex systems of multiple hydraulic fractures, especially when the created hydraulic fracture intersects the natural fracture. It can be mentioned here that the intersection of a hydraulic fracture with a network of natural fractures can also cause post fracture damage. The pre- and post-fracture study conducted by Branagan et al. (1987) showed that water associated with fracturing fluids reduced the relative gas permeability of the natural fractures that were intersected and polymer residue blocked gas flow from the intersected natural fractures.

Figure 1: Idealizations of multi-stranded hydraulic fractures.

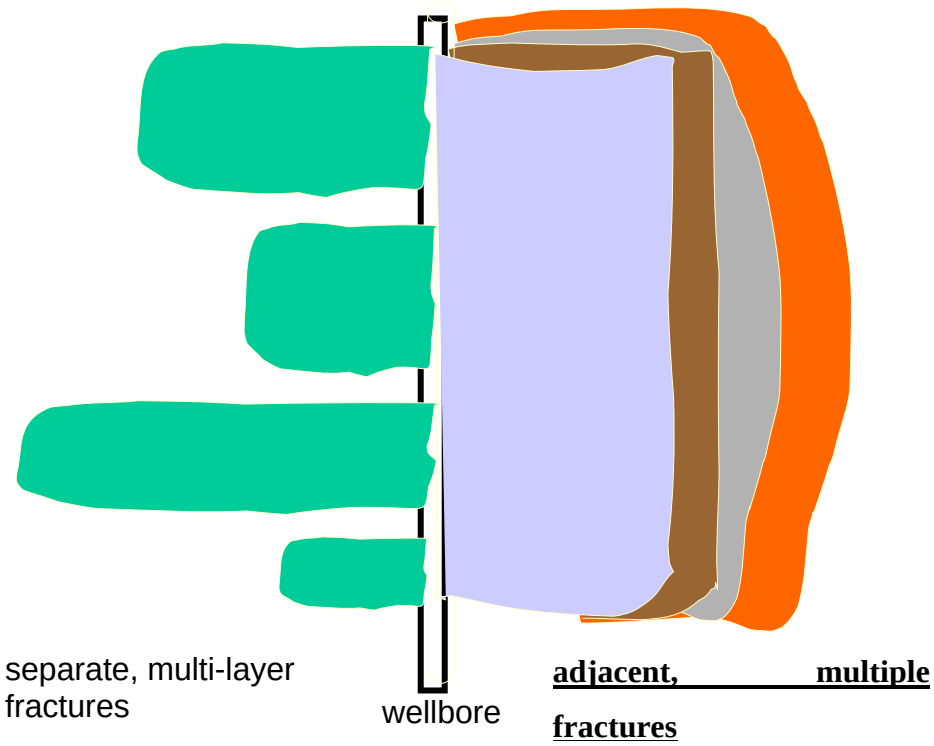

The simultaneous growth of multiple hydraulic fractures is expected to be most pronounced under the following circumstances:

- when large perforated or openhole intervals are stimulated, allowing fractures to propagate into the formation from many different locations along the wellbore;
- when a hydraulic fracture propagates in an area which is intensely naturally fractured;
- when the preferred fracture plane (plane of fracture propagation in the far field) does not coincide with the wellbore orientation.

The main implications of multiple fractures are:

a) significantly increased screenout potential because each individual multiple fracture is narrower than a single fracture would have been,

b) shorter and narrower fractures because the fluid and proppant has to be shared by a number of multiple hydraulic fractures,

c) and higher net pressures because fractures open against each other and compete for fracture width.

In naturally fractured reservoirs, the propagation of multi-stranded fractures may occur wherever a natural fracture intersects the wellbore or is intersected by a growing hydraulic fracture. In naturally fractured reservoirs, therefore, multiple hydraulic fractures are typically initiated and propagated, often in increasing numbers as more natural fractures are intersected by the growing hydraulic fractures. This process is self-reinforcing as the propagation of multiple hydraulic fractures tends to elevate the net fracturing pressure. This in turn makes it easier to start hydraulic fracture propagation at newly intersected natural fractures.

FRACTURE INTERSECTION AND CROSSING

When a hydraulic fracture intersects a joint or other discontinuity at some angle, the hydraulic fracture may propagate across, shear and/or dilate the joint. Blanton (1986) studied the interactions between induced and existing fractures in scaled laboratory experiments for different angles of approach and states of stress. He observed that hydraulic fractures with an approach of 30 degrees to existing fractures tended to open the latter, diverting the fluid and preventing the induced fracture from crossing. Hydraulic fractures at angles of approach of 60 to 90 degrees tend to cross existing fractures when the differential stress is high enough. He stated that initially a natural fracture will arrest an approaching induced fracture because of the very high tensile stresses ahead of the propagating fracture that will open the natural fracture. As the induced fracture propagates into the natural fracture, its tip is blunted thereby arresting its propagation. After the initial arrest, when the fracture has been stopped in both directions, pressure will continue to increase at the points of intersection until either the natural fracture opens or reinitiation occurs on the other side of the natural fracture.

Warpinski and Teufel (1987) observed that in homogenous ash-fall tuff formations, hydraulic fractures diverge considerably from the usual assumption of planar fracture walls. Multi-stranding, fracture meandering, and large-scale surface roughness are common occurrences and in the vicinity of geological discontinuities, the situation is often worse. Frequently there are no planar fracture segments; instead the hydraulic fracture could be better described as a zone of multiple fractures, sometimes 15 to 30 feet wide.

Jeffrey et al. (1987) used a numerical simulator for studying the mechanical interactions of branched or subparallel hydraulic fractures, showing that hydraulic fractures may develop offsets when cross cutting natural fractures. This confirms that in naturally fractured regions, multi-stranding of hydraulic fractures is predominant. Pumping fluid into a fractured rock formation can inflate the natural fractures, and the resulting hydraulic fracture may propagate as a system of parallel to sub-parallel hydraulic fractures with both opening and sliding movement across the fracture surfaces. Alternately, if the natural fractures are more widely spaced, the hydraulic fracture may propagate as a single fracture but interact with natural fractures, one by one, as it approaches the natural fracture. This will offset the hydraulic fracture and cause it to branch out. Experiments conducted by Warpinski et al. (1987) showed that in general, new fractures initiate at the pre-existing joint tips. Some of these fracture strands die out in a short distance while others persist. These fractures divide and coalesce many times along the fracture length. The evolution, scale, and total effect of fracturing depends to a large degree on ancillary parameters like the orientation of the joints with respect to the maximum horizontal stress direction (or fracture orientation). Faults have also exhibited a significant influence on fracture geometry and morphology. Warpinski and Teufel (1987) observed that fractures often terminate near faults and if the hydraulic fracture propagates across a fault, a change in orientation is frequently observed. Invariably this can be

attributed to a change in stresses across the fault and not propagation of the fault plane itself. The fracture usually propagates a short distance across the fault and terminates.

NEAR WELLBORE TORTUOSITY

Near-wellbore fracture tortuosity is a width restriction in the area of a hydraulic fracture that connects the wellbore with the far-field fractures as illustrated in Fig. 2 Aud et al. (1994) have stated that tortuosity can result from:

1. gradual or sharp fracture curvature due to reorientation of the fracture from the plane of initiation towards the preferred fracture plane (plane of far-field fracture growth),
2. sharp fracture curvature due to intersection of the hydraulic fracture with natural or drilling induced fractures,
3. multiple hydraulic fractures that compete for fracture width, and
4. fracture growth along the annulus between the cement and the stiffer casing due to inadequate cementing. Fractures may initiate into the formation away from the perforated interval.

They further state that significant level of tortuosity during fracture treatment greatly increases the risk of a premature screenout due to proppant bridging in the tortuous near-wellbore region.

Figure 2: Near wellbore fracture tortuosity

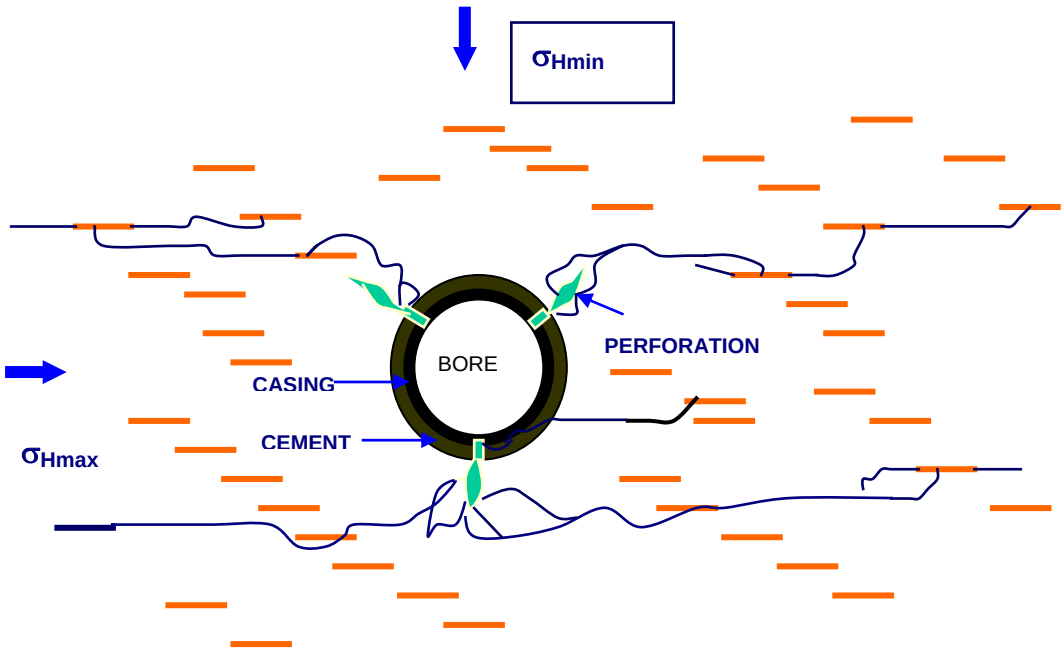

FLUID LEAKOFF & HYDRAULIC FRACTURE BRANCHING:

Fracturing fluid is typically lost into the matrix, but it may be lost into the natural fractures as well. Thus leakoff has to be studied in depth when investigating hydraulic fracturing in naturally fractured reservoirs. The fissure dominated leakoff mechanism varies with in situ stress anisotropy and net pressure. Britt et al. (1994) reviewed several aspects of fluid leakoff in natural fractures that are unique:

1. Nolte and Smith (1979) showed how natural fractures affected net treating pressures and established that treating pressures in excess of the critical pressure generally resulted in premature screenouts. In addition, they showed a qualitative method of identifying natural fractures by evaluating a log-log plot of net treating pressure versus pump time. Their work showed that the net pressure tends to flatten when excessive fluid leakoff to the natural fractures occurs.

2. Mukherjee (1991) showed the stress-sensitive nature of the fluid leakoff and proposed methodology to handle fluid leakoff as a function of net treating pressure. Warpinski (1988) showed that the fluid leakoff to natural fracture

systems can be as much as 50 times greater than matrix leakoff. He further presented the successful application of 100mesh sand as a fluid loss additive in naturally fractured reservoirs to minimize these detrimental effects. This was also shown by Northcutt et al. (1988).

3. Cramer (1991) addressed the excessive fluid loss to natural fractures by reducing net treating pressure, thereby minimizing the leakoff into the fracture system.

Some of the factors that increase leak-off for hydraulic fracturing in naturally fractured reservoirs also adversely affect well performance due to gel damage and/or stress sensitivity.

FRACTURE MODELING

The complexities created by the presence of natural fractures makes building a complete hydraulic fracture model challenging. Pyrak-Nolte (1996) pointed out that fractures in rock primarily influence three physical properties that are of interest to geoscientists and engineers. These are hydraulic conductivity, mechanical stiffness, and the attenuation and/or delay of seismic waves. At a fundamental level, the link between these properties is the geometry of fracture or fracture network. The geometrical properties of a single fracture include the aperture distribution, the spatial distribution of apertures, and surface roughness. For a fracture network, there are additional geometrical properties such as fracture spacing, fracture orientation, spatial correlation among fractures, and interconnectivity of the fractures. Following fracture initiation, additional fluid injection would result in fracture propagation. The geometry of created fractures can be approximated by models that take into account the mechanical properties of the rock, the properties of the fracturing fluid, the condition with which the fluid is injected (rate, pressure), and the stresses and stress distribution in the porous medium.

Ben-Naceur (1989) describes two sets of laws are required necessary for fracture modeling: conservation of momentum, mass and energy, and a propagation criteria.

There are three general families of models, two-dimensional (2D), pseudo-three dimensional (P3D) and, fully three-dimensional (3D) models. In fully three-dimensional models, the fracture propagation is three-dimensional while the fluid flow is 2D. The fracture is discretized, and within each block, calculations are done based on the fundamental laws and criteria for propagation. The fracture is allowed to propagate laterally and vertically depending on the local stress distribution and rock properties, but it is typically forced to maintain a planar geometry. Economides et al. (1989) suggest fractures in horizontal and highly deviated wells may require full 3D modeling, because the fracture initiation, usually aligned with the well trajectory, is likely to be different from the direction of fracture propagation, which must be normal to the minimum, "far-field" stress. Two-dimensional models are attractive because they can be closed-form, analytical expressions, but their assumptions are often too restrictive for accurate fracture modeling. For petroleum engineering applications, two models have been commonly used:

a) For a fracture length much larger than the fracture height, the Perkins and Kern (1961) and Nordgen (1972) or PKN model is an appropriate approximation (Fig. 3).

b) For fracture lengths much less than fracture height, the appropriate model has been presented by Geertsma and de Klerk (1969). This is known as the Khristianovich - Geertsma - de Klerk (KGD) model (Fig. 4).

Figure 3 : CLASSIC PKN MODEL

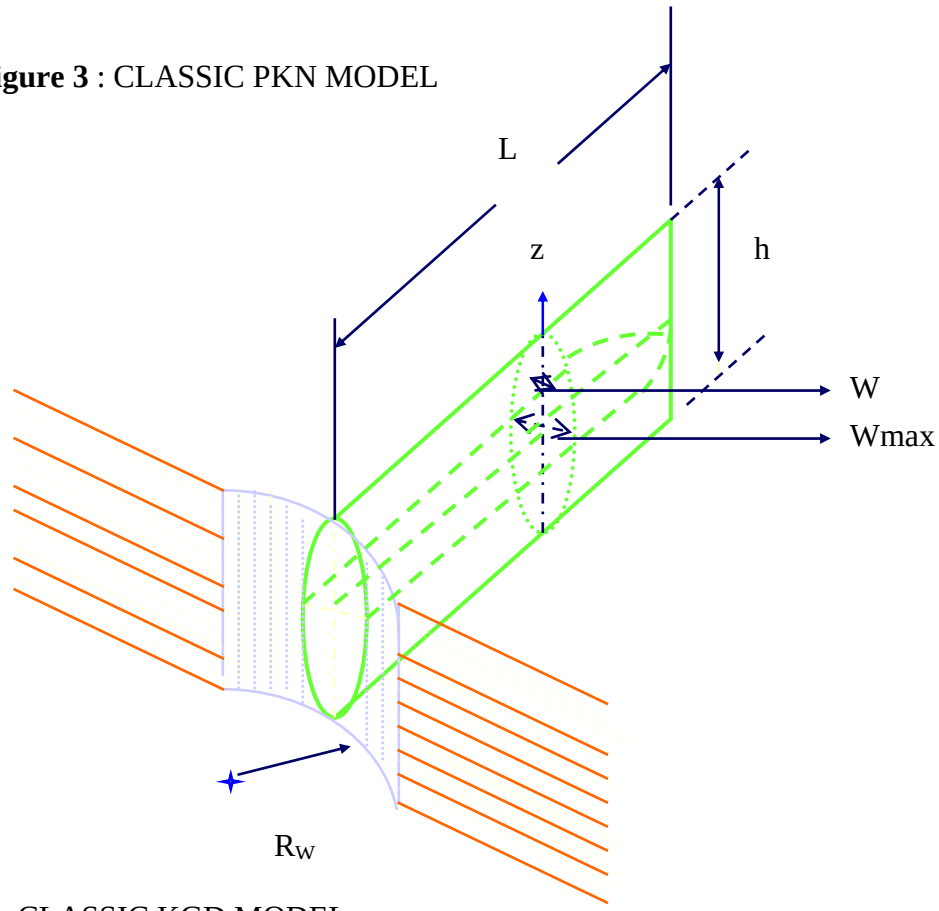

Figure 4 : CLASSIC KGD MODEL

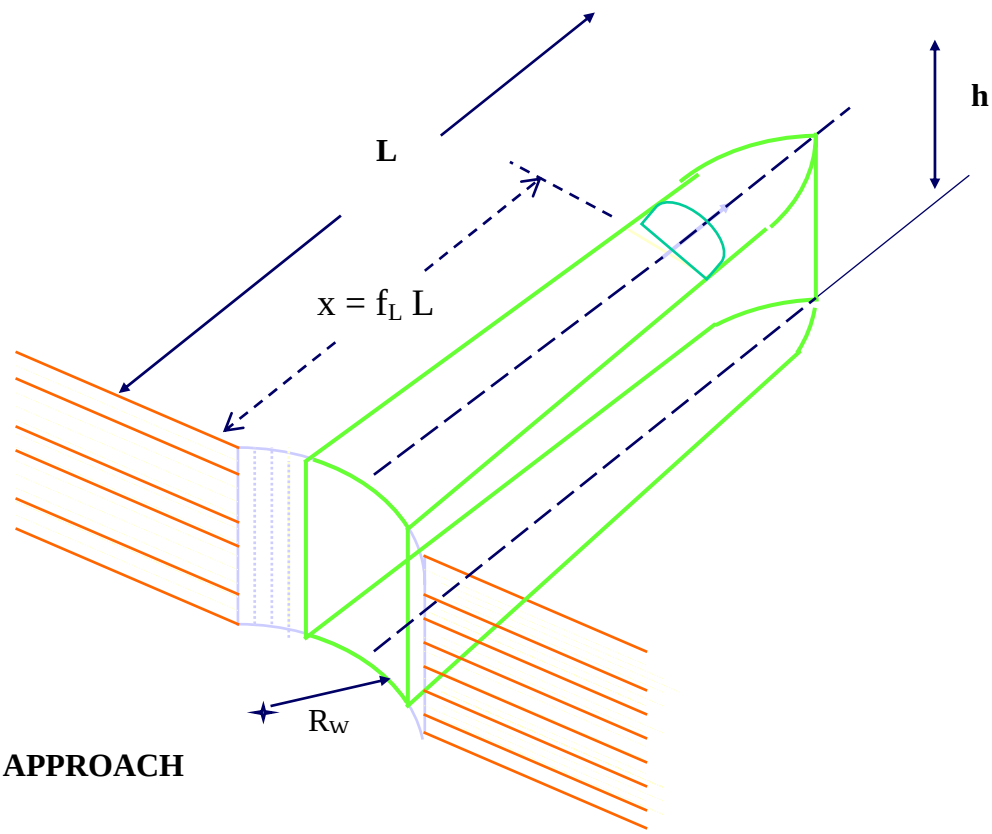

OUR APPROACH

Using a two-dimensional displacement discontinuity model (Olson, 1995), propagation of hydraulic fracture in a naturally fractured reservoir was observed. The limitation was that the hydraulic fracture was treated as a constant pressure crack. Pressure drop is being incorporated into this model by coupling this model with another pseudo 3d model (Wang, 2000) for hydraulic fracture propagation.

The model uses the displacement discontinuity method (Crouch, 1976) to compute fracture opening based on fracturing pressure and in situ stress boundary conditions. The modeled cracks are divided into linear displacement discontinuity elements (dislocations) of constant length over which opening is constant, but adjacent elements can have different opening depending on the net pressure at each element. Elements are added at the fracture tip during propagation. The displacement discontinuity at any given element induces normal and shearing tractions on nearby elements defined as (Crouch and Starfield, 1983; Olson, 1990)

$$\sigma_s^i = A_{ns}^{ij} D_s^j + A_{nn}^{ij} D_n^j \tag{1}$$

$$\sigma_n^i = A_{ss}^{ij} D_s^j + A_{sn}^{ij} D_n^j \tag{2}$$

where σ^i_n and σ^i_s are the normal and shear stress at the ith element due to D^j_n and D^j_s, the normal and shear displacement discontinuity components at the jth element. The coefficient matrix A are called the influence coefficients that define the relationship between displacement discontinuity and stress. Using the principal of superposition, a system of algebraic equations is constructed (Jaegar and Cook, 1979) to give the total stress at the ith element due to displacement discontinuities at all N elements (Crouch and Starfield 1983, Olson 1990)

$$\sigma_n^i = \sum_{j=1}^{N} A_{ns}^{ij} D_s^j + \sum_{j=1}^{N} A_{nn}^{ij} D_n^j \tag{3}$$

$$\sigma_n^i = \sum_{j=1}^{N} A_{ns}^{ij} D_s^j + \sum_{j=1}^{N} A_{nn}^{ij} D_n^j \tag{4}$$

In the above equations, for ‘i’=1 to N we have 2N equations and 2N unknowns, D, given the stress boundary conditions. (Olson, 1990)

The two dimensional displacement discontinuity solution of Crouch (1976) is modified to approximate three dimensional elasticity by multipying the influence coefficient matrix by a correction factor (Wang, 2000), F, defined as

$$F = 1 - x^3 \left[x^2 + \left(\frac{h}{2} \right)^2 \right]^{-3/2} \tag{5}$$

When the distance between the interacting elements, x, is much smaller than the fracture height, h, the correction factor F approaches 1, giving the unaltered 2D solution. Conversely, when the distance between elements is large relative to the height, F tends to zero (Olson, 1995b; Wang, 2000).

Material balance equations are required to incorporate fluid injection into the elastic fracture solution. For a non compressible fluid , the mass conservation equation is (Valko and Economides, 1995)

$$\frac{\partial q}{\partial x} + \frac{2hC_L}{\sqrt{t-\tau}} + 2\frac{\partial h}{\partial t} S_p + h\frac{\partial w}{\partial t} + w\frac{\partial h}{\partial t} = 0 \tag{6}$$

where

$\frac{\partial q}{\partial x}$ - change in flow rate over distance

$q_L = \frac{2hC_L}{\sqrt{t-\tau}} + 2\frac{\partial h}{\partial t} S_p$ - leakoff volume

C_L - fluid loss coefficient

S_p - Spurt loss

τ - time when fracture reaches location x.

$\frac{\partial A}{\partial t} = h\frac{\partial w}{\partial t} + w\frac{\partial h}{\partial t}$ change in cross-sectional area

h - fracture height, and

w - fracture width.

As flow takes place through the fracture, pressure loss occurs. This pressure drop is a function of flow rate and fracture width, height and length. We have considered power law fluid in two cases, a rectangular cross-section and an elliptical cross-section. The pressure drop equation for rectangular cross-section is given by (Valko and Economides, 1995)

$$\frac{\Delta p}{L} = 2^{n+1} k \left(\frac{1+2n}{n} \right)^n q^n h^{-n} w^{-(2n+1)} \tag{7}$$

Pressure drop for elliptical cross-section (with eccentricity =1) is give by (Valko and Economides, 1995)

$$\frac{\Delta p}{L} = \frac{2^{n+5}}{3\pi} \left(\frac{1+2n}{n} \right)^n K q^n h^{-n} w^{-(2n+1)} \tag{8}$$

where k and n are power-law fluid rheology parameters

The fracture propagation direction is obtained using the maximum circumferential stress criterion (Erdogan and Sih, 1963) that states

$$K_I \sin\theta + K_{II}(3\cos\theta - 1) = 0 \tag{9}$$

where θ is the counterclockwise positive angle from the direction of in-plane propagation. K_I is the opening mode stress intensity factor, given by Olson (1990) as a function of boundary element opening displacement discontinuity, D_n, and element length, a, as

$$K_I = \frac{D_n E \sqrt{\pi}}{4\left(1-\nu^2\right)\sqrt{2a}} \tag{10}$$

where E is the Young's modulus and ν is the Poisson's ratio. K_{II} is the shearing mode stress intensity factor (Olson, 1990)

$$K_{II} = \frac{D_S E \sqrt{\pi}}{4\left(1-\nu^2\right)\sqrt{2a}} \tag{11}$$

where D_s is the shearing displacement discontinuity of the boundary element.

ALGORITHM

The approach to the code is illustrated in the flow chart of Figure 5. On the first cycle of a given iteration for a particular time increment, we calculate an elastic width distribution along the fracture assuming constant net pressure from wellbore to tip.

Figure 5: Fracture Propagation Algorithm

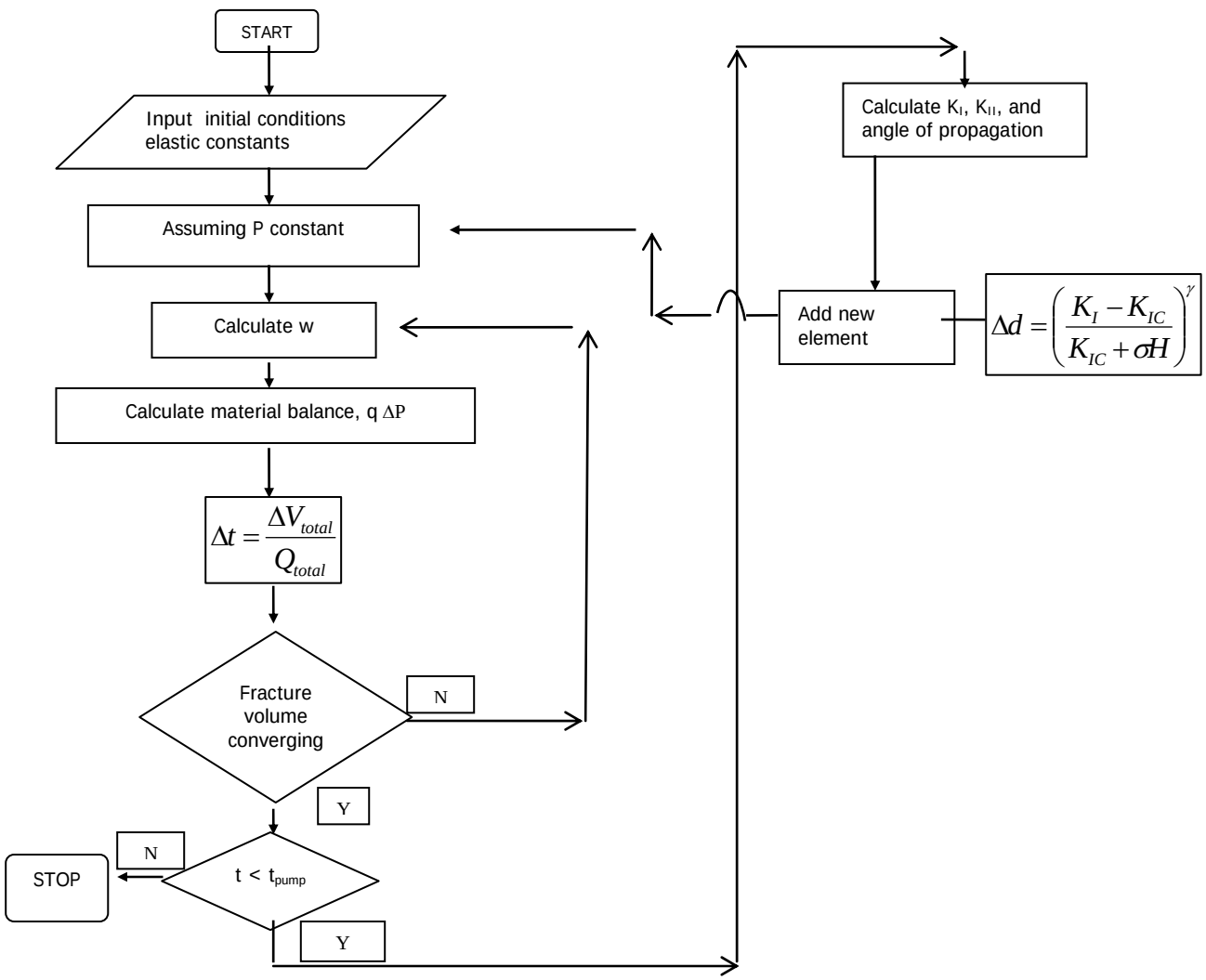

Knowing the change in the fracture volume from the previous time step, ΔV_f, we assume no leak-off and estimate the length of the current time increment, Δt, as

$$\Delta t = \frac{\Delta V_f}{q_{inj}} \tag{12}$$

where q_{inj} is the injection rate at the wellbore. Knowing the width and approximate time increment, we calculate the material balance in each element using equation (6), including leak-off. The consequent pressure drop down each element is computed with either equation (7) or (8). Integrating the leak-off volume over the entire fracture and adding it to the known fracture volume, we can then computer a more accurate *dt* for the current computation cycle. However, as mentioned above, on the first iteration cycle, we assume constant net pressure along the fracture to compute the initial elastic fracture opening for a given time increment. Having computed pressure loss down the fracture, we know that constant pressure is no longer consistent with our material balance, so we recompute the fracture widths given the new fracture pressure distribution. We cycle until the fracture volume converges to a stable value.

COMPUTING FLOW AT BRANCHES

A complicating factor when propagating a hydraulic fracture through a field of natural fractures is computing the flow branching at the point of fracture intersection (Figure 6). If the propagating hydraulic fracture (HF) intersects a natural fracture (NF) at its midpoint, the rate must be split into the two branches of the NF (segment *a* and *b*), designated as Q_{ia} and Q_{ib}. As we iterate through the fracture propagation cycles, the division of the rates to the different branches will depend on the fracture volume changes during a particular timestep as given by

$$\frac{Q_{ia}}{Q_{ib}} = \frac{\frac{\Delta V_{ia}}{\Delta t}}{\frac{\Delta V_{ib}}{\Delta t}} = \frac{\Delta V_{ia}}{\Delta V_{ib}} \tag{13}$$

where ΔV_{ia} and ΔV_{ib} are the elemental fracture volume changes that occur over Δt , the time interval. Continued iteration proceeds as described above, incorporating material balance and leak-off.

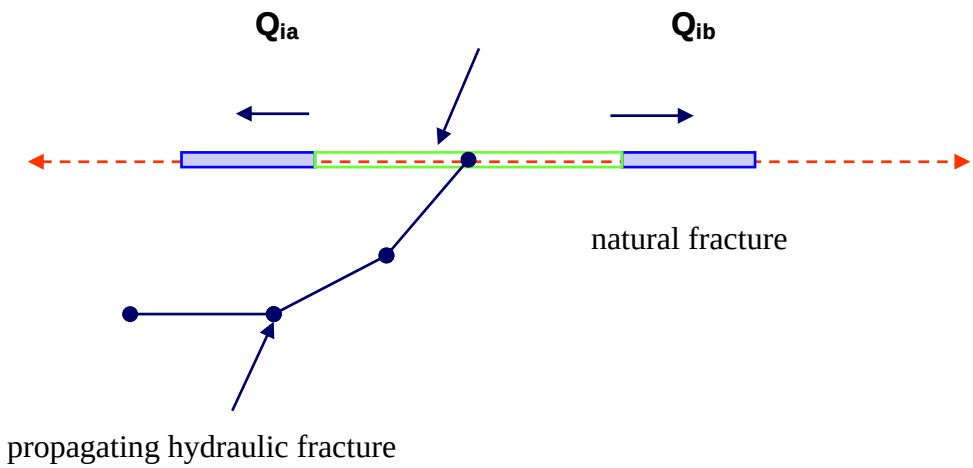

STATUS

We initially tried to modify the single, non-planar fracture propagation code by adding the capability for mutliple, interacting fractures (hydraulic and natural). This resulted in some unanticipated difficulties, so we are now modifying a similar but distinct natural fracture propagation code that already accommodates the simultaneous propagation and mechanical interaction of hundreds of arbitrarily shaped fractures in pseudo-3d (Olson et al., 2001). Our main tasks are to incorporate material balance linked to a central injection point (a wellbore) and to properly divide flow at fracture intersections. The idea is that once the initial hydraulic fracture intersects a pre-existing natural fracture, that natural fracture will take on fluid and ultimately propagate. We are currently working to get code convergence after the first fracture intersection.

REFERENCES

Aud, W.W., Wright, T.B., Cipolla, C.L., Harkrider, J.D., and Hansen, J.T., "The Effect of Viscosity on Near-Wellbore Tortuosity and Premature Screenouts," paper SPE 28492 presented at the 1994 Annual Technical Conference and Exhibition, New Orleans, September 25- 28, 1994.

Ben Naceur, K., "Modeling of Hydraulic Fractures," in Reservoir Stimulation, 2nd ed., M. J. Economides and K. G. Nolte, eds., Prentice Hall, Engelwood Cliffs, NJ, 1989.

Blanton, T.L., "Propagation of Hydraulically and Dynamically Induced Fractures in Naturally Fractured Reservoirs", Unconventional Gas Technology Symposium, of SPE, held in Louisville, May 18-21, 1986.

Branagan, P.T., Cipolla, C.L., Lee, S.J., Yan, L., "Case History of Hydraulic Fracture Performance in the Naturally Fractured Paludal Zone : The Transitory Effect of Damage", Low Permeability Reservoirs Symposium, Denver CO, May 18-19, 1987.

Britt L. K., Hager C. J., and Thompson, J.W., " Hydraulic Fracturing in a Naturally Fractured Reservoir", SPE 28717, paper was prepared for presentation at the SPE International Petroleum Conference & Exhibition of Mexico, 10-13 October, 1994.

Cleary, M. P., Johnson, D.E., Kogsboll, H.H., Owens, K.A., Perry, K.F., de Pater, C.J., Schmidt, H., Tambini, M., "Field implementation of proppant slugs to avoid premature screen-out of hydraulic fractures with adequate proppant concentration," SPE paper 25892, presented at Rocky Mountain Regional/Low Permeability Reservoirs Symposium, Denver CO, Apr 12-14, 1993.

Cramer, D. D.,"Treating Pressure Analysis in The Bakken Formation," SPE 21820, presented at the SPE Low Permeability Reservoirs Symposium, Denver, CO, April 1991.

Crouch, S.L., and Starfield, A.M., "Boundary Element Methods in Solid Mechanics", George Allen Unwin, London, 1983.

Crouch, S.L., "Solution of Plane Elasticity Problems by the Displacement Discontinuity Method," International Journal for Numerical Methods in Engineering, v. 10, p. 301-343, 1976.

Economides, M.J., Hill, A.D., and Economides, C.E., Petroleum Production Systems, 1989.

Elbel, J.L., Piggott, A.R., and Mach, M.G, "Numerical Modeling of Multilayer Fracture Treatments," SPE Permian Basin Oil and Gas Recovery Conference: Midland, TX, 1992.

Erdogan, F., and Sih, G.C., "On the Crack Extension in Plates Under Plane Loading and Transverse Shear," Journal of Basic Engineering, p. 519-527, 1963.

Fast, R.E.; Murer, A.S.; and Timmer, R.S.: "Description and Analysis of Cored Hydraulic Fractures, Lost Hills Field, Kern County, California", SPE 24853, presented at the 1992 Annual Technical Conference and Exhibition of the Society of Petroleum Engineers, Washington, Oct 4-7, 1992.

Geertsma, J. and de Klerk, F., "A Rapid Method of Predicting Width and Extent of Hydraulically Induced Fractures", JPT 1571-1581; Trans., AIME, 246 Dec. 1969.

Hossain, M.M., Rahman, M.K., Rahman, S.S.,: “Hydraulic fracture initiation and propagation: roles of wellbore trajectory, perforation and stress regimes”. Journal of Petroleum Science and Engineering 27(2000) 129-149, March 2000.

Jaeger, J.C. and Cook, N.G.W., Fundamentals of Rock Mechanics, 3rd edition, Chapman and Hall, 1979.

Jeffrey, R.G., Vandamme, L., and Rogers, J.C., “ Mechanical Interactions in Branched or Subparallel Hydraulic Fractures,” SPE 16422, 1987.

Mukherjee,H., Larkin, S. and Kordziel,W.: “Extension of Fracture Pressure Decline Curve Analysis to Fissured Formations”, SPE 21872, presented at the SPE Low Permeability Reservoirs Symposium, Denver, CO, April 1991.

Nolte, K.G. and Smith, M.B. : “Interpretation of Fracturing Pressures,” paper SPE 8297 presented at the 54th Annual Technical Conference and Exhibition, Las Vegas, NV, Sept. 1979.

Nordgren, R.P., "Propagation of a Vertical Hydraulic Fracture", SPEJ 306-314; Trans., AIME, 253, Aug. 1972.

Northcutt, J. C., Robertson, C. J., Hannah, R. R., “State-of-the-Art Fracture Simulation of the Upper Morrow Formation in the Anadarko Basin”, SPE 18260, presented at the 63rd Annual Technical Conference and Exhibition of the Society of Petroleum Engineers, Houston, TX, Oct 2-5, 1988.

Olson, J.E., “Fracture Mechanics Analysis of Joints and Veins,” Dissertation, Stanford University, 1990.

Olson, Jon E., "Fracturing from highly deviated and horizontal wells: numerical analysis of non-planar fracture propagation," SPE Mountain Regional and Low Permeability Meeting, Denver, CO, March 1995.

Olson, J.E., “The Influence of Bed Thickness on Fracture Pattern Geometry: Results from a 3d Mechanical Model”, American Geophysical Union Fall Annual Meeting, San Francisco, December 11-15, 1995(b).

Olson, J. E., Holder, J., Qiu, Y. and Rijken, M., 2001, “Constraining the spatial distribution of fracture networks in naturally fractured reservoirs using fracture mechanics and core measurements,” 2001 SPE Annual Technical Conference and Exhibition, New Orleans, LA, Sept. 30 – Oct. 3, 2001.

Perkins, T. K. and Kern, L. R., "Widths of Hydraulic Fractures", JPT 937-946; Trans., AIME, 222, Sept. 1961.

Pyrak-Nolte, L.J., “Fracture Geometry and Fluid Flow,” The 9th Kongsberg Seminar on Processes at the Fluid-Rock Interface, 1996.

Valko, P. and Economides, M.J., Hydraulic Fracture Mechanics, Wiley and Sons, 1995.

Wang, Xiuping, “Numerical Simulation of Hydraulic Fracturing for Horizontal Wells”, M.S. Thesis, The University of Texas at Austin, December, 2000.

Warpinski, N.R., “Dual Leakoff behavior in Hydraulic Fracturing of Tight, Lenticular Gas Sands,” SPE 18259, presented at the 63rd Annual Technical Conference and Exhibition of the Society of Petroleum Engineers, Houston, TX, Oct 2-5, 1988.

Warpinski N.R., and Teufel L.W., “Influence of Geologic Discontinuities on Hydraulic Fracture Propagation,” JPT, February, 1987.

Warpinski, N.R., Lorenz, J.C., Branagan, P.T., Myal, F.R., and Gall, B.L., “Examination of a Cored Hydraulic Fracture in a Deep Gas Well,” SPE 22876, presented at the 1991 Annual Technical Conference and Exhibition of the Society of Petroleum Engineers, Dallas, TX, Oct 6-9, 1991.

Warpinski, N.R., Moschovidis, Z.A., Parker, C.D., and Abou-Sayed, I.S., "Comparison Study of Hydraulic Fracturing Models: Test Case - GRI Staged Field Experiment No.3", SPE paper 25890 presented at the 1993 SPE Rocky Mountain Regional Meeting and Low Permeability Symposium, Denver, Apr. 26-28, 1993.

PROJECT TITLE #II-9 Control Schemes for Intelligent Multilateral Wells

PRINCIPAL INVESTIGATOR: A. D. Hill
RESEARCH SCIENTIST: D. Zhu
GRADUATE STUDENT: Weidong Chen

SUMMARY

The objectives of this project were to develop a mathematical model of multilateral well performance, and to implement the model into a computer software, and to use the model to predict and optimize multilateral well deliverability.

We have developed a comprehensive model in IWP Phase I and Phase II. The model calculate the flow profile along each lateral, the flow profile from each lateral, and the total flow rate, as functions of tubinghead pressure for multilateral wells. The multilateral well deliverability model couples the calculations of inflow to each lateral, pressure drop behavior in each lateral, and pressure drop in the main wellbore. It finds the equilibrium producing point for commingled production in multilateral wells by iteration (referring IWP Annual Report, Project #9, 2000 and 2001).

The model also predicts life-cycle performance for single-phase incompressible reservoirs by material balance. With material balance calculate, the flow rate decline in individual lateral, and the total accumulation production can be estimates, thus, this model can optimize well performance for different completion schemes. The examples presented in previous report show that well configurations affect multilateral well performance significantly.

In the last year of study in multilateral well, we have focused on the crossflow phenomenon in commingled multilateral production. Crossflow is defined as that the fluid from one lateral flows into another lateral instead of flow up to surface during the production period. It is caused by pressure difference in different reservoir compartments, and multiphase flow in pipes also plays an important role in crossflow. It disturbs the reservoir condition unexpectedly, results in a reduced surface production, and therefore

should be avoid in commingled wells. There are two ways to eliminate crossflow, one is to apply intelligent well system (downhole measurement and control), and the other is to produce at appropriate surface pressure (mostly a lower surface pressure). Both methods to eliminate crossflow need a model to predict the flow distribution and detect the conditions that result in crossflow. Our multilateral model can be used for this purpose. In our publication (SPE 75250), we discussed this problem with a field example. This problem should be studied in depth, and a two-phase reservoir model will be highly appreciated for the study.

The software generated from this project, UTMWP, is released for testing and field applications. The interface of UTMWP makes the input part self-explained and user-friendly. The output of the software includes the flow rate distribution from each lateral and the total flow rate as functions of surface pressure digitally and graphically, and low rate and pressure distribution along each lateral digitally.

Publications from this project

8. Chen, W, Zhu, D. and Hill, A. D.: "Development of Multilateral Well Deliverability Model," Presented at proceedings of ETCE/OMAE2000 joint conference energy for the new Millenium, New Orleans, LA, U.S.A., 14-17, February 2000.
9. Chen, W. D., Zhu, D. and Hill, A. D.: "A Comprehensive Model of Multilateral Well Deliverability," SPE 64751, presented at the SPE International Oil and Gas Conference and Exhibition, Beijing, China, 7-10 November, 2000.
10. Zhu, D. and Hill, A. D.: "Optimizing Performance of Intelligent Wells," 2001 SPE Forum Series in Europe III, Ste. Maxime, France, September 23 - 28, 2001.
11. Zhu, D. Hill, A. D., and Landrum, W. R.: "Evaluation of Crossflow Effects in Multilateral Wells," SPE 75252, will be presented at the SPE/DOE Thirteenth Symposium on Improved Oil Recovery held in Tulsa, Oklahoma, 13–17 April 2002.

PROJECT TITLE, #II-10 Completion Performance in Horizontal Laterals

PRINCIPLE INVESTIGATOR: Dr. A. D. Hill

RESEARCH SCIENTIST: Dr. D. Zhu

GRADUATE STUDENT: Kenji Furui

A RIGOROUS FORMATION DAMAGE SKIN FACTOR AND RESERVOIR INFLOW MODEL FOR A HORIZONTAL WELL

In this study, we developed a new analytical model[1] for formation damage skin factor and the resulting reservoir inflow that includes the effect of reservoir anisotropy and damage heterogeneity. We assumed that the shape of the damaged region perpendicular to the wellbore is based on the pressure equation[2] for an anisotropic medium, and is thus circular near the well and elliptical far from the well. This assumption gives an exact and analytical skin factor even for a small penetration of damage. By assuming the radial or elliptical flow geometry near the well and taking the integration of the local flow over the entire well length, the new model can account for any distribution of damage along the well. The new skin factor model can be easily incorporated into any existing model of reservoir inflow for a horizontal well.

We also present a new reservoir inflow equation for a damaged parallelepiped-shaped reservoir drained by a horizontal well. This equation shows that the ratio of the reservoir thickness to the drainage length perpendicular to the well is a very important factor for determining the influence of formation damage on horizontal well productivity because linear flow becomes dominant for a thin reservoir. The larger the ratio of thickness to drainage length perpendicular to the well axis, the larger the influence of near-well formation damage on well productivity.

Our models give a simple, analytical expression for determining the impact of formation damage on horizontal well production. The details of derivation of our equations and the examples are presented in our SPE paper[1].

A NEW SKIN FACTOR MODEL FOR PERFORATED HORIZONTAL WELLS

Objectives

Perforation skin models for vertical wells have already been presented in many papers. However, they are not directly applicable to a horizontal well because the reservoir anisotropy in a horizontal well creates complex plane flow geometry normal to the well which alters the flow efficiency of a perforated completion. In this work, we present a new skin factor model developed for a cased, perforated horizontal well. From our observations, the 2-D plane flow skin, $s_{2D,}$ and the wellbore blockage effect, $s_{wb,}$ greatly depend on the magnitude of the permeability anisotropy and the perforation angle measured from a horizontal plane. Our model is based on the conventional perforation skin model for a vertical well presented by Karakas & Tariq[3].

Our perforation skin model is a semianalytical solution that is correlated with finite element simulation results. To take into account the effect of reservoir anisotropy, a coordinate transformation[4] into an equivalent isotropic space is applied.

One of the great advantages of introducing a skin model for a perforated well is that we can directly consider the wellbore blockage effect and additional skin factors such as the impacts of formation damage and perforation damage (rock compaction around perforation). The modified perforation skin model developed here gives optimized perforation conditions and helps us to understand complex flow geometry in a horizontal perforated well. Using an accurate finite-element simulator, we also show a verification of the model.

Problem Description

Fig. 1 shows the key parameters of a perforated completion presumed in this study. In formations with no significant formation damage or perforation damage, the perforation skin, s_p, will be a function of;

(1) The number of perforations per plane, m (analogous to angular phasing, θ, in Karakas & Tariq's model[3])

(2) Perforation length, l_p

(3) Perforation radius, r_p

(4) Perforation shot density, n_s (or spacing between perforations along a well, h)

(5) Index of anisotropy, I_{ani} ($=\sqrt{k_H / k_V}$)

(6) Wellbore radius, r_w.

(7) Perforation orientation, α (the azimuth angle measured from the horizontal plane)

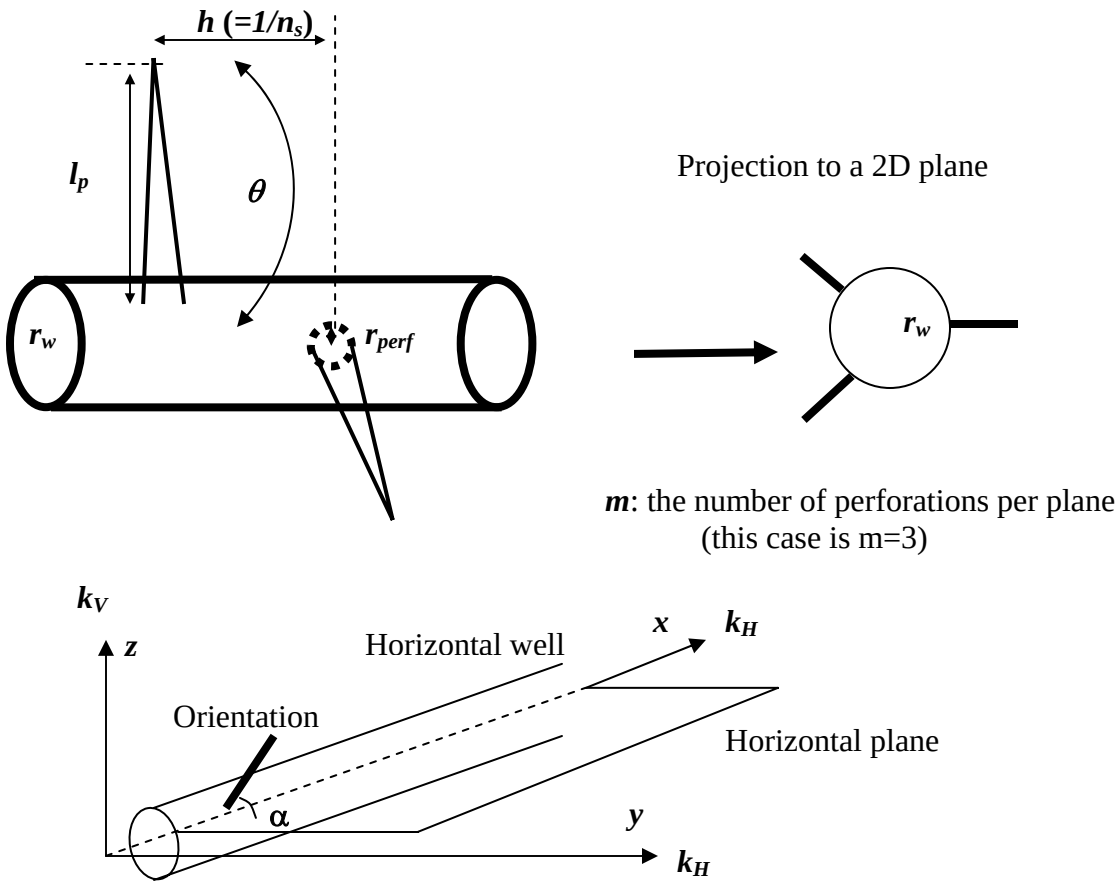

Fig. 1 Perforation geometry

The most important and significant difference between perforation skin models for vertical and horizontal wells is the perforation orientation α. For a horizontal well completed in an anisotropic reservoir, the perforation skin factor is strongly influenced by α, especially in highly anisotropic reservoirs. In this study, we considered four types of commonly used perforation phasings as shown in Fig. 2.

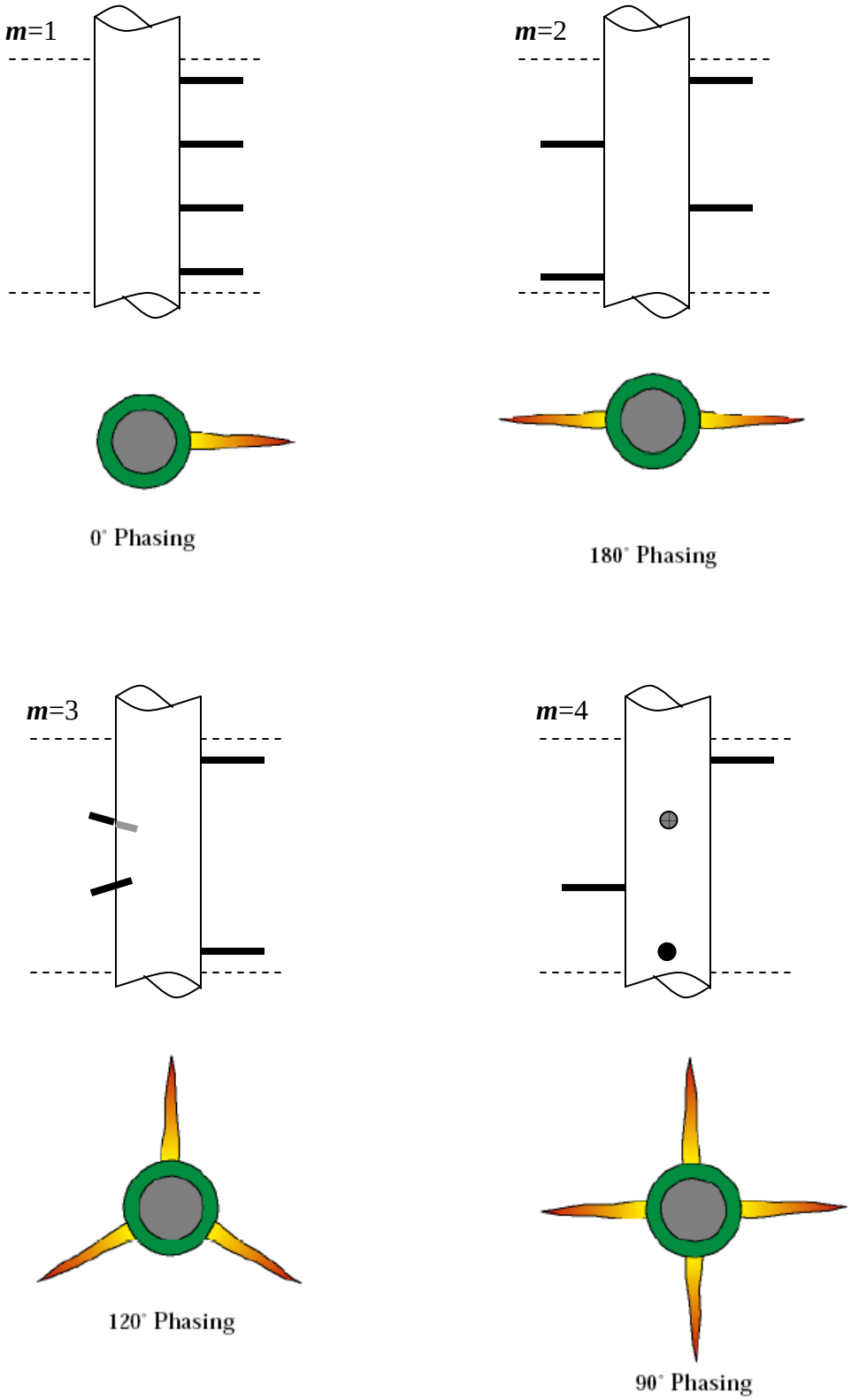

Fig. 2 Perforation phasings modeling

Theoretical Considerations

The mathematical solution of the problem requires that a number of assumptions be made concerning the porous media, the perforations and the fluid.

1. A single, incompressible fluid is flowing. The flow is viscous and steady-state.
2. The effect of gravity is negligible.
3. Horizontal well
4. All fluid enters the formation across the drainage boundary of the well. Fluid is produced only through the casing perforations.
5. The anisotropy ratio, k_H/k_V, is constant throughout the reservoir.
6. At some radius beyond the wellbore, the effect of the perforations is not felt. Beyond this radius, flow is radial (or elliptical in anisotropic reservoirs) and can be described by the normal logarithmic distribution.
7. The pressure drops inside the perforations are assumed to be negligible.

The perforation skin factor, s_p, indicates the relative efficiency of a perforated well, compared with an ideal openhole completion. The steady-state flow into a perforated well for radial flow can be described by

$$q_p = \frac{2\pi k h_t \Delta p}{\mu[\ln(r_e / r_w) + s_p]} \tag{1}$$

Where r_e is the reservoir drainage radius. Mathematically, the problem reduces to that of solving the diffusivity equation in Cartesian coordinates for a specific set of boundary conditions. The finite element method (FEM) was used to solve the equations. FEM simulation results are used to estimate the perforation skin factor by solving the following equation,

$$\frac{q_p}{q_o} = \frac{\ln(r_e / r_w)}{\ln(r_e / r_w) + s_p} \tag{2}$$

where q_p is a productivity estimated by a FEM simulator under a particular perforation condition and q_o is the ideal openhole completion with the same fluid and formation properties as the simulation. The simulations are executed for different perforation conditions and generate the perforation skin database to find appropriate correlation equations.

Following Karakas & Tariq's model[3], we decided to divide the perforation skin into three components; the 2-D plane flow skin, s_{2D}; the wellbore blockage skin, s_{wb}; and the 3-D convergence skin factor, s_{3D}. The total perforation skin factor is then given by

$$s_p = s_{2D} + s_{wb} + s_{3D} \tag{3}$$

s_{2D} is a skin factor simulated under 2-D plane flow geometry without the existence of the wellbore. The plane flow is considered as infinite perforation shot densities and neglecting any convergence effect in the direction along the wellbore (x-direction). This skin factor can be negative or positive depending on the perforation conditions and the reservoir anisotropy.

s_{wb} is also estimated for a 2-D plane flow geometry. Because of the distortion of the flow into the perforation, the perforation skin simulated with the wellbore, s_c is expected to be comparatively greater than s_{2D}. The difference of skin factor between them is s_{wb}, that is,

$$s_{wb} = s_c - s_{2D} \tag{4}$$

The wellbore blockage skin will be positive for any perforation condition. The sum of s_{2D} and s_{wb} is interpreted as a limit of the perforation skin factor for infinite perforation shot density.

For low perforation shot densities, the flow geometry around a perforation becomes extremely complicated. Therefore, a 3-D FEM analysis is required. According to the Karakas & Tariq's work[3], the 3-D wellbore blockage effect may be approximated by s_{wb} defined by the 2-D analysis for practical perforation conditions. A skin factor estimated by the 3-D FEM simulation, s_c, is used to estimate an additional flow convergence effect into the perforations in the x-direction, denoted by s_{3D}. s_{3D} can be approximately given by

$$s_{3D} = s_c - s_{2D} \tag{5}$$

This is also positive for any perforation condition.

FEM Simulation

An analytical treatment of the flow problem in the perforated completion is extremely difficult because of the complicated flow geometry. In addition, for a horizontal well, the reservoir anisotropy may make the flow geometry more complicated. The finite element technique is a powerful approach for evaluating the fluid flow in porous media in complex geometries. The first step in application of the method is to divide the region of interest into elements. The elements should be graded in shape and size to follow boundaries and also should be small enough to assure the accuracy of the numerical solution. A piecewise approximation to the solution is then imposed for each element and flux equilibrium equations are developed at a discrete number of points within the network of finite elements.

We have developed a finite element code that allows the elements to model steady-state fluid flow in porous media. The pressure distribution for this element is obtained from the numerical solution of the following diffusivity equation:

$$\frac{\partial}{\partial x}\left(k_{xx}\frac{\partial p}{\partial x}\right)+\frac{\partial}{\partial y}\left(k_{yy}\frac{\partial p}{\partial y}\right)=0 \qquad \text{for a 2-D problem} \qquad (6)$$

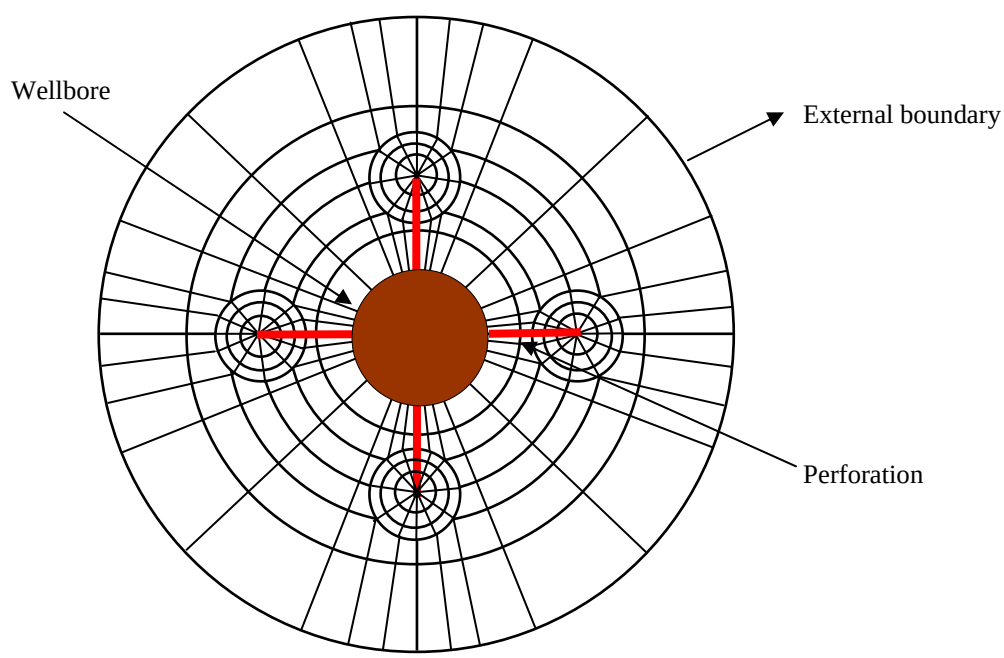

Fig. 3 Finite element mesh for modeling 2-D flow

Fig. 3 shows a grid layout used in the 2-D simulation for m=4 (90° phasing). The number of nodes and their distribution were modified according to perforation parameters (the maximum number of elements were around 6000 elements). The formation is represented by 2-D triangular and rectangular elements. Both types are quadratic. Constant pressure boundary conditions are applied to the nodes on the outer boundary and the perforations for the evaluation of steady-state flow.

In this study, the wellbore radius and the external radius were 0.5 ft and 660 ft. The other parameters were chosen as follows:

l_p ; 0.0556, 0.125, 0.2143, 0.3333, 0.5, 0.75, 1.1667, 2.0, and 4.5 ft

I_{ani} ; 1,2,3,4,5,6,7,8,9, and 10

α ; 0, 15, 30, 45, 60, 75, and 90 degree

m ; 1, 2, 3, and 4

The total number of simulation runs is 2520.

A NEW SKIN FACTOR MODEL FOR PERFORATED HORIZONTAL WELLS

2-D Plane Flow Skin, s_{2D}, in an Anisotropic Medium

The general 3D problem is not easily amenable to analytical treatment. To obtain a tractable solution, we decided to study first the simpler 2D problem, the solution of which essentially forms the basis for the solution of the full 3D problem. In the 2D analysis, we ignore any flow caused by perforation density. Therefore, the flow into the perforations is considered independent of a coordinate parallel to the wellbore. Analysis of the plane flow into perforations is important because:

(1) The solution of the 2D analysis gives the limit of the perforation skin factor for infinite perforation shot density for a particular perforation condition.

(2) It can establish a basis for the solution of the general 3D problem and gives insight into the relative importance of various perforation parameters in well productivity.

For most practical perforation lengths and well radii, the perforation diameter (assuming negligible vertical flow) would have minimal effect on well productivity. Therefore, under these conditions, s_p would essentially be controlled by m, l_p, I_{ani}, α